the plant journal

SEB SOCIETY FOR EXPERIMENTAL BIOLOGY

The Plant Journal (2021) **107**, 448–466 doi: 10.1111/tpj.15301

Ride to cell wall: Arabidopsis XTH11, XTH29 and XTH33 exhibit different secretion pathways and responses to heat and drought stress

Monica De Caroli, Elisa Manno, Gabriella Piro* and Marcello S. Lenucci

Dipartimento di Scienze e Tecnologie Biologiche e Ambientali, Università del Salento, Lecce 73100, Italy

Received 6 October 2020; revised 16 April 2021; accepted 23 April 2021; published online 1 May 2021.
*For correspondence (e-mail gabriella.piro@unisalento.it).

SUMMARY

The xyloglucan endotransglucosylase/hydrolases (XTHs) are enzymes involved in cell wall assembly and growth regulation, cleaving and re-joining hemicellulose chains in the xyloglucan–cellulose network. Here, in a homologous system, we compare the secretion patterns of XTH11, XTH33 and XTH29, three members of the *Arabidopsis thaliana* XTH family, selected for the presence (XTH11 and XTH33) or absence (XTH29) of a signal peptide, and the presence of a transmembrane domain (XTH33). We show that XTH11 and XTH33 reached, respectively, the cell wall and plasma membrane through a conventional protein secretion (CPS) pathway, whereas XTH29 moves towards the apoplast following an unconventional protein secretion (UPS) mediated by exocyst-positive organelles (EXPOs). All XTHs share a common C-terminal functional domain (XET-C) that, for XTH29 and a restricted number of other XTHs (27, 28 and 30), continues with an extraterminal region (ETR) of 45 amino acids. We suggest that this region is necessary for the correct cell wall targeting of XTH29, as the ETR-truncated protein never reaches its final destination and is not recruited by EXPOs. Furthermore, quantitative real-time polymerase chain reaction analyses performed on 4-week-old Arabidopsis seedlings exposed to drought and heat stress suggest a different involvement of the three *XTH*s in cell wall remodeling under abiotic stress, evidencing stress-, organ- and time-dependent variations in the expression levels. Significantly, *XTH29*, codifying the only XTH that follows a UPS pathway, is highly upregulated with respect to *XTH11* and *XTH33*, which code for CPS-secreted proteins.

Keywords: XTH, UPS, EXPO, cell wall trafficking, heat stress, drought stress, *Arabidopsis thaliana*.

INTRODUCTION

The physico-chemical properties of the primary cell wall in angiosperm strongly affect organ growth and adaptation to a changing environment full of stimuli. Cell wall architecture responds to a general model in which crystalline cellulose microfibrils are embedded in an amorphous network of polymers (hemicelluloses, pectins and structural proteins) and secreted enzymes (Cosgrove, 2005). The integrated activity of these enzymes prompts a coordinated, selective and dynamic remodeling of the complex polymeric network and mediates all events implied in cell expansion and growth, as well as many physiological processes, including fruit ripening, organ abscission and biotic/abiotic stress responses (Rose *et al.*, 2002). In this context, xyloglucans (XGs) and the enzyme family of endotransglucosylase/hydrolases (XTHs), involved in *in muro* polysaccharide metabolism, have been proposed to play a significant role in the assembly, disassembly and remodeling of the cellulose/XG network (Miedes *et al.*, 2013; Nishitani and Vissenberg, 2006; Thompson and Fry, 2001).

The XGs are hemicellulosic polysaccharides of variable length and side-chain patterns constituting the major polymers of the growing primary cell walls of dicots and non-commelinoid monocots (Fry, 1989; Gibeaut *et al.*, 2005; Hayashi, 1989; Schultink *et al.*, 2014). For a long time XGs were thought to cover most of the cellulose microfibrils, preventing their association with one another and simultaneously acting as the major load-bearing tether between adjacent microfibrils (Cosgrove, 2001; Fry, 2004; Scheller and Ulvskov, 2010). Recent studies report that only a minority of XGs interact with cellulose, forming coil-shaped fine spots resembling 'biomechanical hot spots'

that control wall extension (Park and Cosgrove, 2012; 2015; Wang *et al.*, 2013), and that binding preferentially occurs at the hydrophobic surface of cellulose (Cosgrove, 2018; Zheng *et al.*, 2018).

The XGs are also covalently linked to pectins (Popper and Fry, 2008; Thompson and Fry, 2001) and proteoglycans (i.e. the arabinoxylan pectin arabinogalactan protein, APAP1) (Tan *et al.*, 2013); significantly, their absence alters cellulose biosynthesis and cellulose microfibril patterning, supporting the role of cellulose–XG interactions in determining wall structure (Xiao *et al.*, 2016).

The XTHs may act as XG hydrolases and/or XG endotransglucosylases (XETs), mediating both the integration of newly secreted XGs into the wall and the remodeling of pre-existing wall XGs (Eklöf and Brumer, 2010; Rose *et al.*, 2002; Thompson and Fry, 2001). These activities generally imply a homo-transglycosylation reaction involving XGs as donor and acceptor substrates; however, hetero-transglycosylating activity between different types of carbohydrate polymers has been reported in Arabidopsis, *Hordeum vulgare* (barley) and *Equisetum* (Fry *et al.*, 2008; Herburger *et al.*, 2020; Hrmova *et al.*, 2007; Mohler *et al.*, 2013; Shinohara *et al.*, 2017; Simmons and Fry, 2017; Simmons *et al.*, 2015).

Specific reviews resume the recent advances on XTH structure, function, reaction mechanism, biochemistry and phylogenesis (Cosgrove, 2005; Eklöf and Brumer, 2010; McGregor *et al.*, 2017; Mellerowicz *et al.*, 2008; Rose *et al.*, 2002); nevertheless, several key aspects on the function and role of XTHs still need to be clarified. Among other factors, the secretion route has scarcely been considered.

Cell wall proteins that contain a signal peptide (SP) are synthesized in the endoplasmic reticulum (ER) and directed to the apoplast through the endomembrane system, following conventional protein secretion (CPS). In plants, the presence of CPS-independent pathways has been reported and is referred to as unconventional protein secretion (UPS). Different types of UPS exist and involve either ER N-terminal SP-lacking proteins (leaderless secreted proteins, LSPs) or SP-containing proteins but, in both cases, their secretion bypasses the Golgi. UPS may also occur through vesicular and non-vesicular transport. Non-vesicular transport involves endomembrane compartments such as vacuoles, multivesicular bodies and exocyst-positive organelles (EXPOs) that fuse directly with the plasma membrane and release their cargo in the apoplast (Davis *et al.*, 2016; Ding *et al.*, 2014; Robinson *et al.*, 2016; Wang *et al.*, 2017).

The presence of an N-terminal SP was predicted for all 33 XTHs identified in Arabidopsis (Ndamukong *et al.*, 2009), although an updated version of the SignalP 5.0 server predicted its absence for XTH29. The leading role of SP for correct entry into the secretory route was clearly demonstrated for several XTHs. The 24-amino-acid N-terminal sequence of Arabidopsis endoxyloglucan transferase A1 (EXGT-A1, now *At*XTH4) was recognized as the signal liable for ER targeting and, ultimately, apoplastic secretion by heterologous expression of the GFP-tagged fragment in Bright Yellow-2 (BY-2) *Nicotiana tabacum* (tobacco) suspension-cultured cells (Yokoyama and Nishitani, 2001a; 2001b). Using the same approach, the putative N-terminal SPs of several *Zea mays* L. (maize) and *Diospyros kaki* L. (persimmon) XTHs (*Zm*XTH1, *Dk*XTH1, *Dk*XTH2, *Dk*XTH6 and *Dk*XTH8), fused to the GFP and transiently expressed in onion cells, were shown to enter the secretory pathway and eventually label the cell wall, similarly to the corresponding full-length XTH-GFP constructs. Accordingly, their fluorescent SP-truncated forms did not localize in the secretory pathway and showed the same behavior of the soluble GFP used as the control (Genovesi *et al.*, 2008; Han *et al.*, 2016a; 2016b; 2015). In contrast to the above reported XTHs, *Dk*XTH7 was predicted to lack SP and appeared dispersed throughout the cell, similarly to the SP-truncated forms (Han *et al.*, 2016a). No direct analyses were performed on the putative N-terminal SP of an XTH from *Populus euphratica* (*Pe*XTH), nevertheless the construct *Pe*XTH-GFP labeled the cell wall and the Hechtian strands of onion plasmolyzed cells, indicating that the protein enters the ER and is secreted to the apoplast, possibly through the CPS pathway (Han *et al.*, 2013). An original role was reported for the N-terminal SP of XTH31, interpreted to be sufficient to confer plasma membrane localization and, therefore, possibly functioning as a plasma membrane-targeted SP (Zhu *et al.*, 2012). Plasma membrane localization was also suggested for XTH17, but no emphasis was placed on the potential role of its predicted N-terminal SP as no fluorescence was detected when the sequence was fused to GFP and transiently expressed in onion epidermal cells (Zhu *et al.*, 2014).

In this article, we analyzed the secretion pattern of three members (XTH11, XTH33 and XTH29) of the *Arabidopsis thaliana* XTH family, by expressing their GFP/RFP-tagged forms in Arabidopsis cotyledons. We show that XTH11 and XTH33 reach their final localization through the CPS pathway, whereas XTH29 moves towards the apoplast through the UPS pathway, probably mediated by EXPOs. We also report a different response of the three XTHs to drought and heat stress in the root and aerial parts of Arabidopsis seedlings.

RESULTS

On the basis of bioinformatic predictions (SignalP 5.0 server, http://www.cbs.dtu.dk/services/SignalP/; TMpred server, https://embnet.vital-it.ch/software/TMPRED_form.html), XTH11, XTH33 and XTH29 were selected for the presence/absence of characterizing motifs: (i) the presence of an SP (XTH11 and XTH33); (ii) the presence of a transmembrane (TM) domain (XTH33); and (iii) the

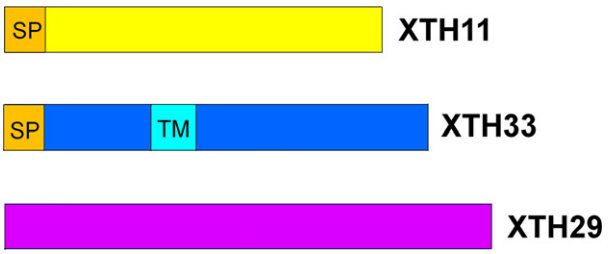

Figure 1. Schematic representation of the xyloglucan endotransglucosylase/hydrolases (XTHs) analyzed. SP, signal peptide; TM, transmembrane domain.

absence of ab SP (XTH29) (Figure 1). The fluorescent variants of the three XTHs were constructed by fusing the respective encoding cDNAs to *gfp*. The fluorescent tag was linked to the C terminus, as none of the three XTHs is predicted to have the ω site of the glycosylphosphatidylinositol (GPI) anchor addition (predGPI software; http://gpcr2.Biocomp.unibo.it/predgpi/). The resulting chimeras, XTH11-GFP, XTH33-GFP and XTH29-GFP (Figure S1), were transiently expressed in Arabidopsis cotyledon epidermal cells and observed by laser scanning confocal microscopy.

XTH11 and XTH33 move through the Golgi stacks and reach the cell wall and the plasma membrane, respectively

XTH11-GFP labeled the ER, continuous to the nuclear envelope, and small punctate structures colocalizing with the ER and Golgi markers RFP-HDEL and ST52-mCherry, respectively (Nelson *et al.*, 2007) (Figure 2a–f). The confocal observations and the colocalization quantitative parameters (Figure 2c,f; Table S1) are consistent with the involvement of the conventional pathway in chimera secretion. To better discern the fluorescent-labeled organelles, confocal images at different scanning depths were acquired: cell walls and vacuoles were captured at the equatorial plane, whereas the other organelles were captured at more superficial confocal planes. XTH11-GFP also clearly labeled the cell walls (Figure 2g), as confirmed by colocalization with the cell wall protein *Phaseolus vulgaris* polygalacturonase-inhibiting protein 2 (PGIP2) fused to RFP (PGIP2-RFP; De Caroli *et al.*, 2011a) (Figure 2g–i), the absence of colocalization with the plasma membrane marker (pm-rk) (Nelson *et al.*, 2007) in plasmolyzed cells with respect to normal conditions (mock treatment) (Figure 2j–l compared to Figure S2a–c) and the immunolocalization of the chimera (approximately 56.5 kDa) in the isolated cell wall protein fraction (Figure 2m). Significantly, the native form of XTH11 was also immunolocalized in the cell wall (Figure S3a), showing the same behavior of the fluorescent tagged chimera.

Similar to XTH11-GFP, the transiently expressed XTH33-GFP labeled the ER of Arabidopsis cotyledonal cells and punctiform Golgi stacks, as verified by colocalization with the corresponding RFP-HDEL and ST52-mCherry markers (Figure 3a–f). Green fluorescence, merging with the red signal of PGIP2-RFP, was clearly detectable at the equatorial plane (Figure 3g–i), indicating the presence of the chimera in the cell wall. Nonetheless, upon plasmolysis of Arabidopsis cotyledons, co-expression studies with pm-rk, although confirming the association of XTH33-GFP with the cell wall, also showed the simultaneous presence of several green, fluorescent dots labeling discrete plasma membrane domains (Figure 3j–l, mock treatment in Figure S2d–f). These observations agree with those reported by Ndamukong *et al.* (2009), who identified XTH33 as a TM protein in tobacco epidermal cells. Western blot analyses confirmed the presence of XTH33-GFP in both the plasma membrane and the cell wall (Figure 3m). Remarkably, upon sodium dodecyl sulfate polyacrylamide gel electrophoresis (SDS-PAGE) a mobility shift of the XTH33-GFP extracted from the isolated membrane and cell wall fractions was observed, possibly indicative of protein cleavage. The apparent molecular weight of the cell wall-associated chimera was indeed substantially lower than that of the membrane-bound XTH33-GFP (approximately 45 and 60 kDa, respectively). Moreover, a similar pattern was revealed with an anti-XTH antibody in Arabidopsis cotyledons transformed with the native form of XTH33 (Figure S3b), demonstrating that protein cleavage was not artifactual. Two additional bands (approximately 33 and 15 kDa) were also visible in the membrane protein fraction, probably matching, respectively, the entire and hydrolyzed forms of XTH33 still associated to plasma membrane.

To confirm that XTH33 was cleaved at the plasma membrane, two new constructs (secGFP-XTH33 and XTH33-RFP) were generated, with GFP and RFP fused to the N and C termini of the protein, respectively. Co-expression and colocalization analyses showed both chimeras labeling the cell periphery (Figure 4a–c); however, after plasmolysis, the green and red tags overlapped at discrete dots on the

Figure 2. Expression of XTH11-GFP in Arabidopsis cotyledon epidermal cells.
XTH11-GFP labels the endoplasmic reticulum (ER) and Golgi stacks colocalizing with their respective markers RFP-HDEL (a–c) and ST52-mCherry (d–f). In the equatorial plane, XTH11-GFP highlights the cell wall (g), colocalizing with cell-wall marker PGIP2-RFP (h, i). Plasmolyzed epidermal cells co-expressing XTH11-GFP and the plasma membrane marker pm-rk shows the chimera in the cell wall (j–l). Western blot of the soluble (SOL), membrane (MEM) and cell wall (CW) protein fractions extracted from epidermal cells expressing XTH11-GFP (m). Overlap coefficient (OC, after Manders) and *R* (Pearson's correlation coefficient) values are reported in each merged image. Statistical data are reported in Table S1. Bands were revealed using an anti-GFP antibody. Scale bars: 20 μm (a–l).

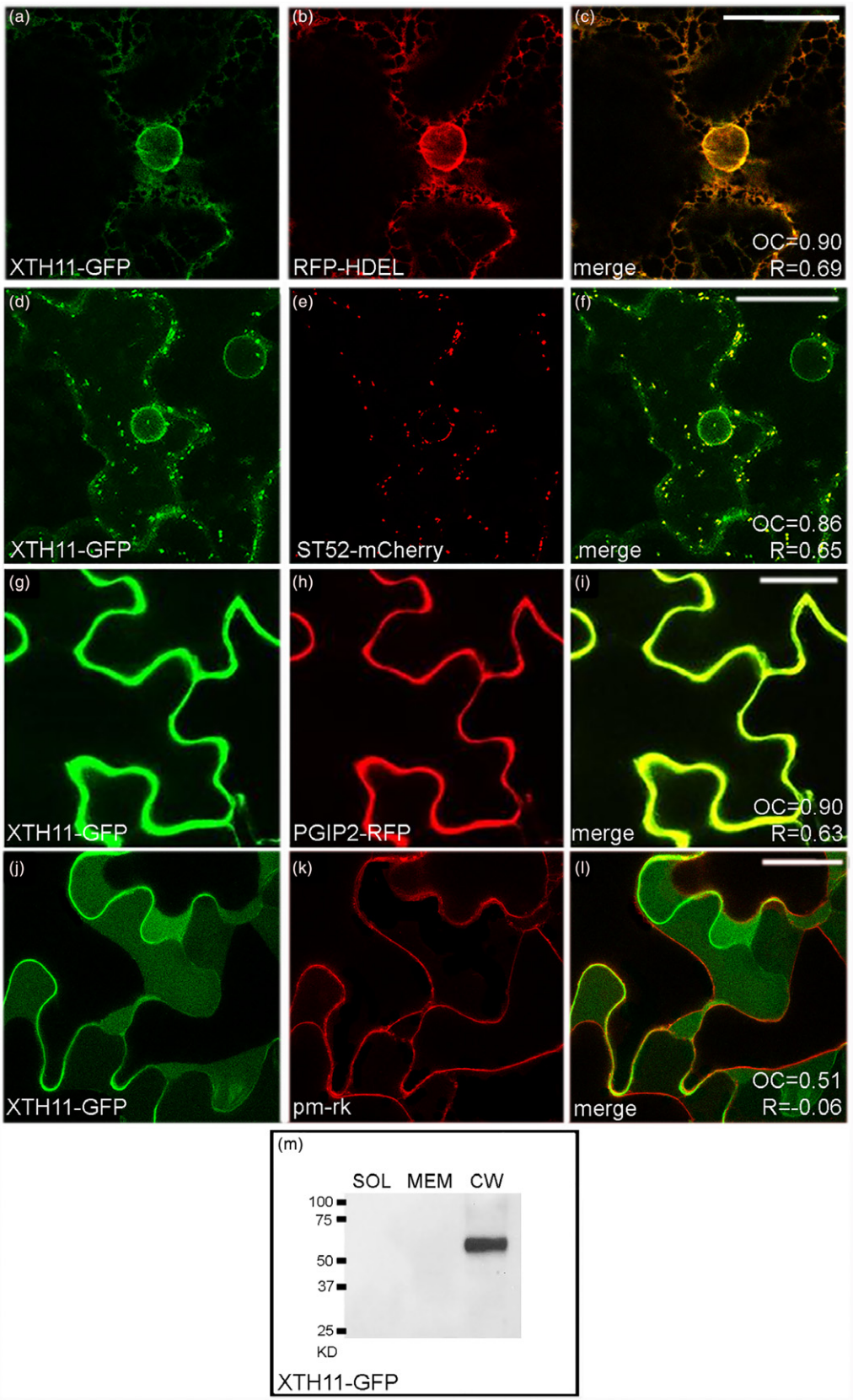

plasma membrane, whereas cell walls fluoresced exclusively red (Figure 4d–f), probably as a result of the hydrolytic release of the RFP-tagged C-terminal domain of XTH33 in the cell wall (Figure 4g). In this regard, it is useful to clarify that XTH33 is assumed to be a type-2 TM protein, with the N-terminal domain in the cytosol and the C-terminal domain in the wall (Figure S4). Indeed, the catalytic domain of the protein, as well as the cysteine residues and the XET-C terminal extension region, follow the TM domain and face the apoplast, where they perform their functions (Ndamukong *et al.*, 2009). This agrees with our observation that cleavage of C-terminally tagged RFP results in a cell-wall RFP signal. Based on the known sequence of the 310 aa of the whole protein and the theoretical molecular weight (approximately 18 kDa) of the released XTH33 C-terminal domain, we used the COMPUTE PI/MW tool (http://web.expasy.org/compute_pi/) to estimate the approximate size of the apoplastic fragment. The size of the apoplastic fragment was estimated to be approximately 160 aa, indicating that protein cleavage occurs near the 150th aa, downstream of the TM domain (90–109 aa) and the conserved catalytic site (116–125 aa) (Ndamukong *et al.*, 2009), which remains associated with the plasma membrane (Figure S4).

XTH29 reaches the cell wall through an unconventional secretion pathway

The cell wall was the final destination of XTH29-GFP: in fact, it colocalized with PGIP2-RFP (Figure 5a–c); did not overlap with pm-rk after the plasmolysis of cotransformed cotyledons (Figure 5d; mock treatment in Figure S2g–i); and was detected as a band of the expected molecular weight (approximately 68 kDa) in the fraction of cell wall proteins (Figure 5e) also in the native form (Figure S3c). Despite this, XTH29-GFP had a secretion pattern that substantially differed from the other XTHs analyzed. XTH29-GFP labeled the nucleoplasm but not the ER and Golgi stacks, in which they appeared to be excluded as no signal overlap was detected with the specific organelle markers (RFP-HDEL and ST52-mCherry, respectively) (Figure 5f–k). To compare directly the different pattern of XTH29 and XTH11, the red variant of XTH29 (XTH29-RFP) was constructed and co-expressed with XTH11-GFP. According to our previous observations, a red-fluorescent nucleoplasm was clearly distinguishable and delimited by the nuclear envelope labeled green by XTH11-GFP (Figure 5l,m), corroborating the entry of XTH11 in the ER and the exclusion of XTH29. Moreover, both chimeras were colocalized at the cell wall (Figure 5n).

Besides nucleoplasm and cell walls, XTH29-RFP labeled small cytosolic punctate structures, frequently observed close to the plasma membrane (Figures 6a and S5). These compartments colocalized with the GFP-tagged Arabidopsis exocyst subunit Exo70 homolog E2 (Exo70E2-GFP), a marker for EXPO (Figure 6b,c) (Wang *et al.*, 2010). To discern more precisely the position of these small structures, XTH29-RFP and Exo70E2-GFP cotransformed Arabidopsis cotyledons were subjected to plasmolysis. Under these conditions, other than in the cytosol, fluorescent punctate structures, labeled with both XTH29-RFP and Exo70E2-GFP, were observed within the extracellular space between the cell wall and the retracted plasma membrane (Figure 6d–g). Similar compartments were first described in plasmolyzed transgenic tobacco BY-2 and Arabidopsis cells expressing Exo70E2-GFP, and interpreted as EXPO-released single-membrane vesicles, relying also on the weaker fluorescence intensity compared with double-membrane EXPOs (Wang *et al.*, 2010). Based on the hypothesis of a possible involvement of EXPOs in the sequestering and trafficking of XTH29-RFP, the fluorescent pattern superimposed with the transmitted light image of the plasmolyzed cell, observed in Figure 6(g), may be schematically represented as in Figure 6(h). It has been reported that Exo70E2 overexpression promotes EXPO formation in plant cells (Ding *et al.*, 2014). Consistently, the average number of XTH29-RFP labeled punctate structures in each epidermal cell increased from 7 ± 3 to 55 ± 10 when Exo70E2-GFP was co-expressed. EXPOs are assumed to be unrelated to autophagosomes in physiological conditions (Wang *et al.*, 2010), and thus XTH29 turnover should occur independently of autophagic processes. In accordance, no colocalization was observed when Exo70B1-GFP, a specific marker of autophagosomes (Kulich *et al.*, 2013), and XTH29-RFP were co-expressed in Arabidopsis cotyledons (Figure S6). Furthermore, XTH11-RFP and XTH33-RFP did not show colocalization with Exo70E2-GFP (Figure S7).

When endotransglucosylase (XET) activity was assessed *in vitro* by the dot blot assay (Fry, 1997) on wild-type and transformed Arabidopsis cotyledons, quantifiable signals were detected in all samples, with those constitutively overexpressing each of the three XTHs or the corresponding GFP-tagged forms under the cauliflower mosaic virus (CaMV) *35S* promoter showing much more intense fluorescence than the wild type (Figure S8a). The variation of XET activity, calculated as pixel intensity percentage relative to wild type (Figure S8b), was above 630% in all transformed samples, indicating that the overexpression of native and GFP-tagged XTHs not only leads to the synthesis of functional enzymes, but also strongly increases the XET activity compared with untransformed cotyledons.

Brefeldin A affects XTH11 and XTH33, but not XTH29, secretion

Brefeldin A (BFA) susceptibility is commonly used to distinguish CPS from UPS, as the two pathways are, respectively, sensitive or insensitive to the drug (Robinson *et al.*, 2016; Zhang *et al.*, 2011). In our experiments, BFA clearly perturbed the secretion pattern of both XTH11-GFP and

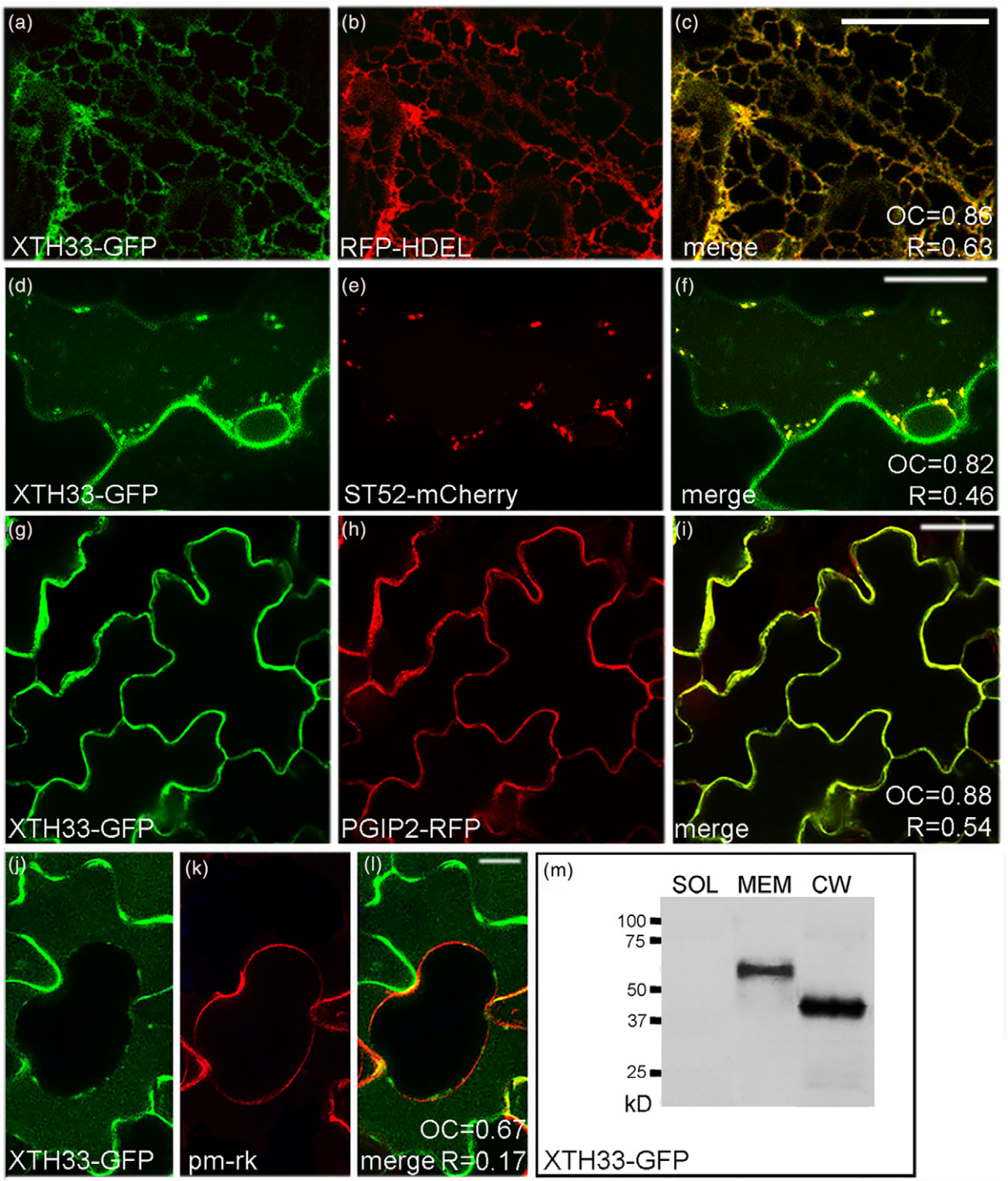

Figure 3. Expression of XTH33-GFP in Arabidopsis cotyledon epidermal cells.
XTH33-GFP is visible in the endoplasmic reticulum (ER) and in the Golgi, where it is colocalized with ER (RFP-HDEL) (a–c) and with Golgi (ST52-mCherry) markers (d–f). (g–i) Co-localization of XTH33-GFP and the cell wall marker PGIP2-RFP. In plasmolyzed cells, XTH33-GFP is detected both in the cell wall and in some discrete dots at the plasma membrane (j), colocalizing with the plasma membrane marker pm-rk (k, j). Western blot of the soluble (SOL), membrane (MEM) and cell wall (CW) protein fractions extracted from epidermal cell expressing XTH33-GFP (m). Overlap coefficient (OC, after Manders) and *R* (Pearson's correlation coefficient) values are reported in each merged image. Statistical data are reported in Table S1. Bands were revealed using anti-GFP antibody. Scale bars: (a–i) 20 μm; (j–l) 5 μm.

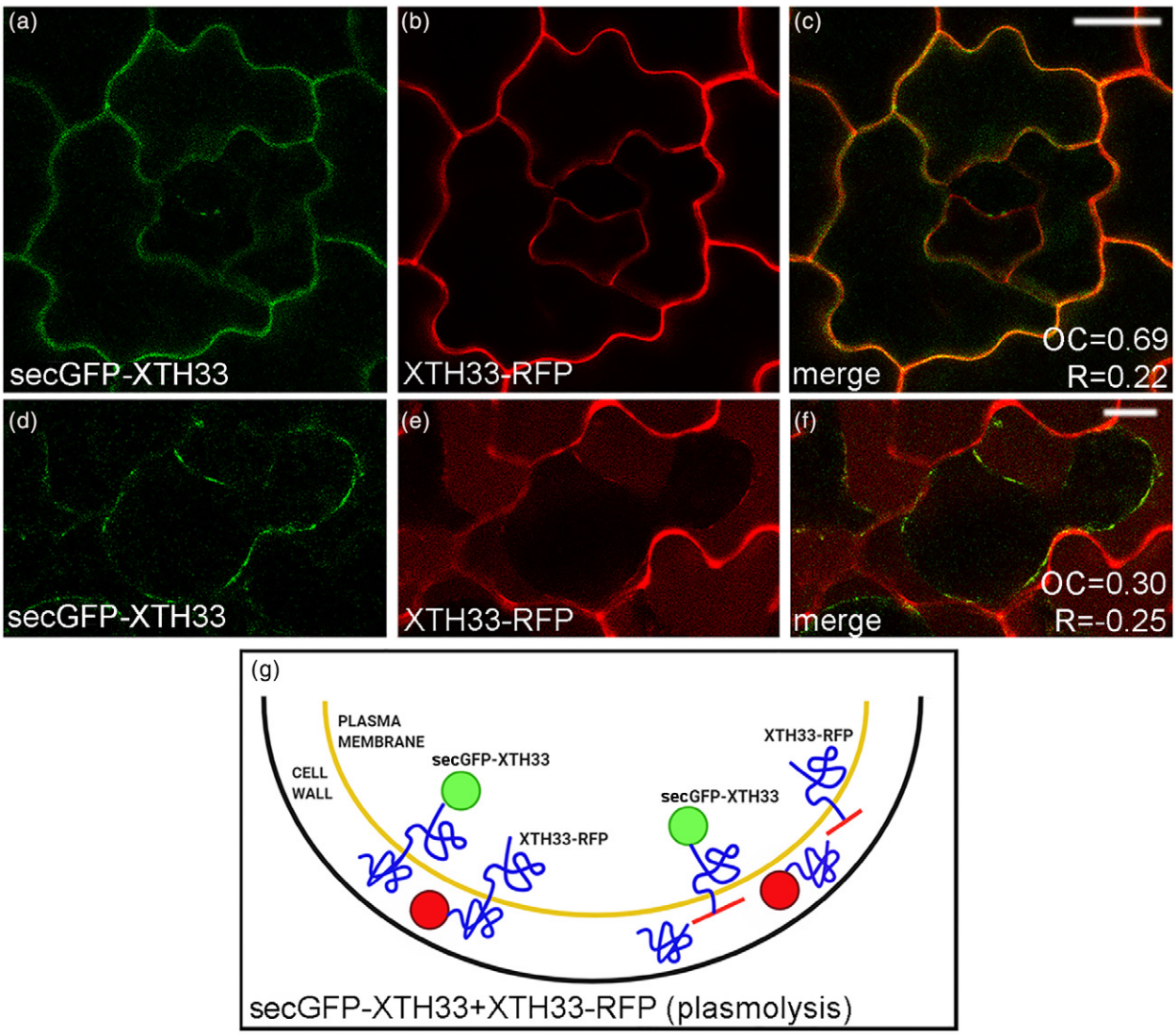

Figure 4. XTH33 is hydrolyzed at its C terminus and this fragment ends up on the cell wall.
(a–c) Co-localization of the chimeras secGFP-XTH33 and XTH33-RFP. (d–f) Plasmolyzed cells cotransformed with secGFP-XTH33 and XTH33-RFP. (g) Graphic representation of the hydrolysis of the N- and C-fluorescent tagged chimeras. Overlap coefficient (OC, after Manders) and *R* (Pearson's correlation coefficient) values are reported in each merged image. Statistical data are reported in Table S1. Scale bars: (a–c) 20 μm; (d–f) 5 μm.

XTH33-GFP. In fact, 30 min after drug administration, the punctate appearance of the Golgi apparatus, labeled by both chimeras and colocalizing with ST52-mCherry (Figure 7a–c, g–i), was lost in favor of the formation of BFA compartments (Figure 7d–f, j–l). In contrast, no change occurred in the distribution pattern of XTH29-GFP in the presence of BFA (Figure 7m,p), despite clear evidence for perturbation in Golgi organization, labeled by ST52-mCherry (Figure 7n,o,q, and r). Control tests with DMSO without BFA did not show any effect (Figure S9). Taken together, the results fully support a CPS route for XTH11 and XTH33 and a UPS route for XTH29, which lacks a canonical SP, and as a result is insensitive to BFA.

XTH29, depleted of the C-terminal 45-amino-acid domain, does not reach the cell wall and is not recognized by EXPOs

To identify the putative domain involved in the recognition and sequestration of XTH29 by EXPOs, XTH29 was aligned (https://blast.ncbi.nlm.nih.gov/Blast.cgi) with the Arabidopsis protein *S*-adenosylmethionine synthetase 2 (SAMS2), demonstrated to follow an EXPO-mediated exocytosis pathway (Wang *et al.*, 2010). Despite that the total alignment score between XTH29 and SAMS2 was very low (<40%), the XTH29 region between 325 and 334 aa shared 50% identity with the 235–244 aa of the SAMS2 domain.

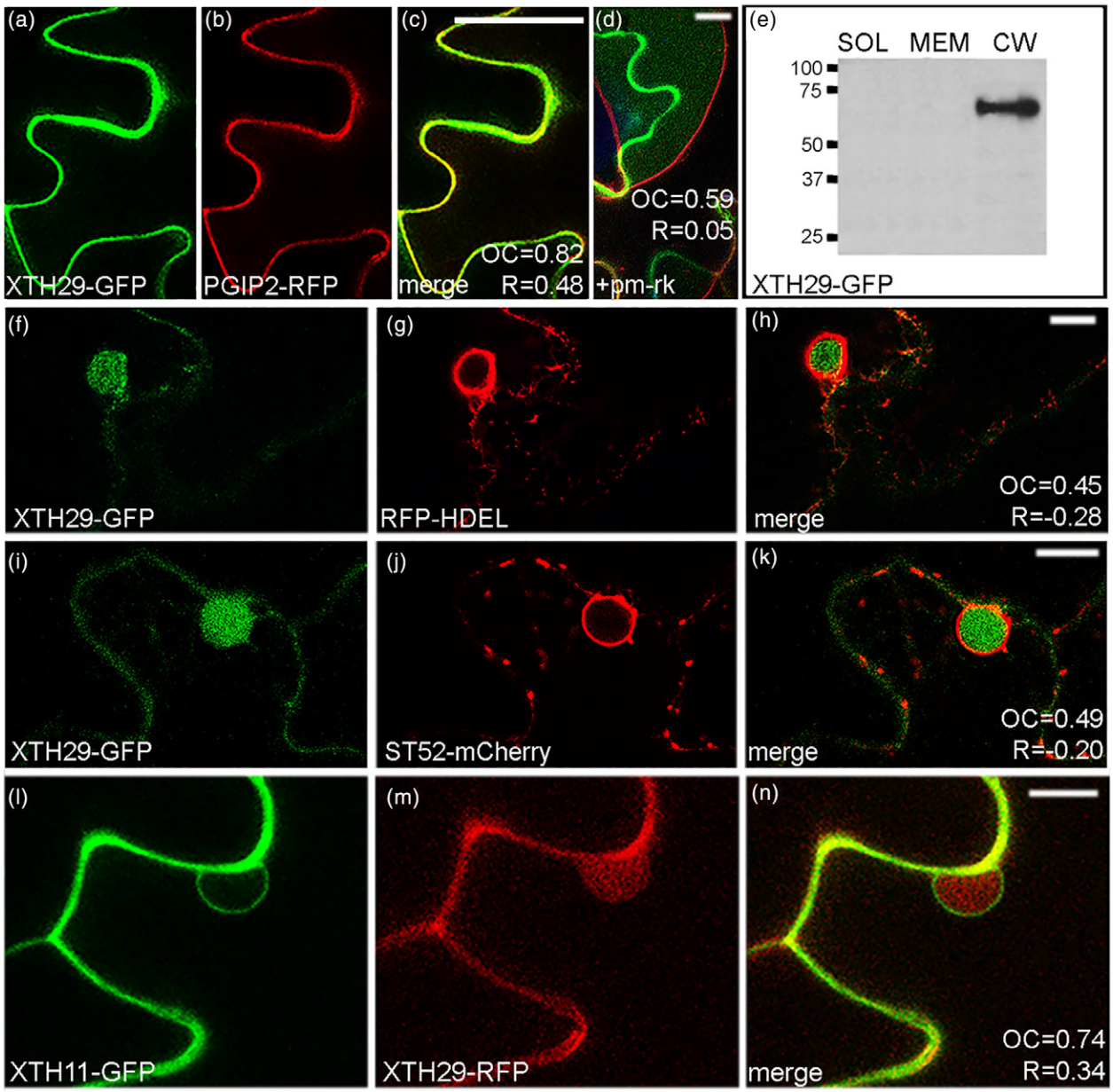

Figure 5. XTH29-GFP reaches the cell wall, bypassing the endoplasmic reticulum (ER) and the Golgi.
(a) XTH29-GFP labels the cell wall. (b, c) Colocalization of XTH29-GFP and the cell wall marker PGIP2-GFP. (d) Plasmolyzed cells cotransformed with XTH29-GFP and pm-rk. (e) Western blot analysis shows the presence of XTH29-GFP in the cell wall protein fraction extracted from epidermal cells expressing XTH29-GFP. XTH29-GFP colocalizes neither with the ER marker RFP-HDEL (f–h) nor with the Golgi marker ST52-mCherry (i–k). (l–n) Co-expression of XTH11-GFP and XTH29-RFP. Overlap coefficient (OC, after Manders) and *R* (Pearson's correlation coefficient) values are reported in each merged image. Statistical data are reported in Table S1. Scale bars: (a–c) 20 μm; (d, f–n) 5 μm.

This sequence was found to be part of an extra-terminal region (ETR, approximately 45 aa), distinctive for a restricted number of XTHs (XTH27, 28, 29 and 30), located outside the functional C-terminal domain (XET-C) present in all XTHs (Johansson *et al.*, 2004) (Figure S10). Thus, the GFP-fluorescent ETR truncated form of XTH29 (XTH29T-GFP) and the RFP-fluorescent fragment (F) covering the last 45 aa (RFP-45aaF) were constructed (Figure S1) and transiently expressed in Arabidopsis cotyledons.

XTH29T-GFP exhibited a typical cytosolic fluorescent pattern, labeling both scattered cytoplasm and nucleoplasm (Figure 8a), with no overlapping with ER and Golgi markers (Figure S11). But, in contrast to XTH29-GFP, the truncated form was never observed in the wall and no colocalization was obtained when it was co-expressed with XTH29-RFP (Figure 8a–d). Confocal observations were confirmed by Western blot analyses of the proteins extracted from XTH29T-GFP transformed cotyledons. Indeed, the

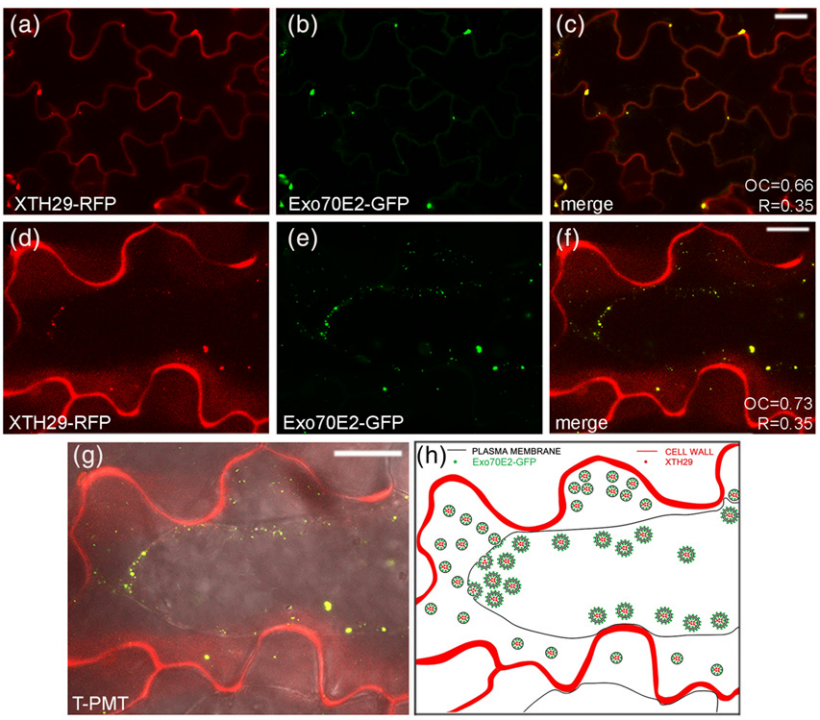

Figure 6. Co-localization of XTH29-RFP and Exo70E2-GFP.
Arabidopsis cotyledon epidermal cells co-expressing (a) XTH29-RFP and (b) Exo70E2-GFP; (c) merged. (d–f) Plasmolyzed cotyledon epidermal cells co-expressing XTH29-RFP and Exo70E2-GFP. (g) Transmitted light detector (T-PMT) image. (h) Graphic representation of panel g: XTH29-RFP (●) is sequestered by exocyst-positive organelles (EXPOs), marked by Exo70E2-GFP (●) in the inner and outer membranes. Overlap coefficient (OC, after Manders) and *R* (Pearson's correlation coefficient) values are reported in each merged image. Statistical data are reported in Table S1. Scale bars: (a–c) 20 μm; (d–g) 5 μm.

XTH29T-GFP band was found in the fraction of cytosolic soluble proteins, but not in the cell wall or the membrane fractions (Figure 8e). Moreover, no red fluorescent punctae were visible in the XTH29T-RFP transformed cotyledons, even after a long incubation period (>72 h) or co-expression with Exo70E2-GFP (Figure 8f–h). Similarly, RFP-45aaF strongly labeled the nucleoplasm, whereas no punctate structures and apoplast were labeled after prolonged observations (Figure S12). Altogether, the results indicate that the 45-aa ETR domain is necessary, but not sufficient, for the correct targeting of XTH29 towards the cell wall and to prompt protein sequestration into the EXPOs.

XTH11, *XTH33* and *XTH29* show different responses to drought and heat stress

The different secretion patterns of XTH11, XTH33 and XTH29 are possibly related to their distinct involvement in specific physiological responses. To verify this hypothesis, we monitored the expression levels of the three isoforms in the roots and aerial part (shoots, epicotyl and leaves) excised from 4-week-old Arabidopsis seedlings subjected to drought or heat stress. In response to drought stress, the *XTH*s analyzed exhibited distinct expression patterns also in terms of organ specificity (Figure 9a; Table S2). Compared with control (unstressed) seedlings, *XTH11* expression in the aerial part did not show any significant change, neither after 2 nor 4 h of stress; increased expression (log2 fold change of between 2 and 4) was, instead, evident in the roots already after 2 h. *XTH33* was drastically downregulated (log2 fold change of between −4 and −7) by drought in the aerial part, but not in the roots, where the fold change was not significant. In the roots, *XTH29* was upregulated (log2 fold change of >4) after 2 h, but downregulated (log2 fold change of between −2 and −4) after 4 h of stress. No significant variation in the expression of *XTH29* was, instead, observed in the aerial part. An organ-dependent variability in the expression of *XTH* genes was also evident in response to heat stress (Figure 9b; Table S2). After 2 and 4 h at 42°C, *XTH11* expression was strongly upregulated in the roots (log2 fold change of between 4 and 7), but not in the aerial part. *XTH33* was upregulated in the roots (log2 fold change of between 6 and 2) and downregulated in the aerial part (log2 fold change of between −5 and −4). *XTH29* was upregulated in both roots (log2 fold change of >6) and aerial parts (log2 fold change of >4), but with different timing (after 2 and 4 h of heat stress, respectively).

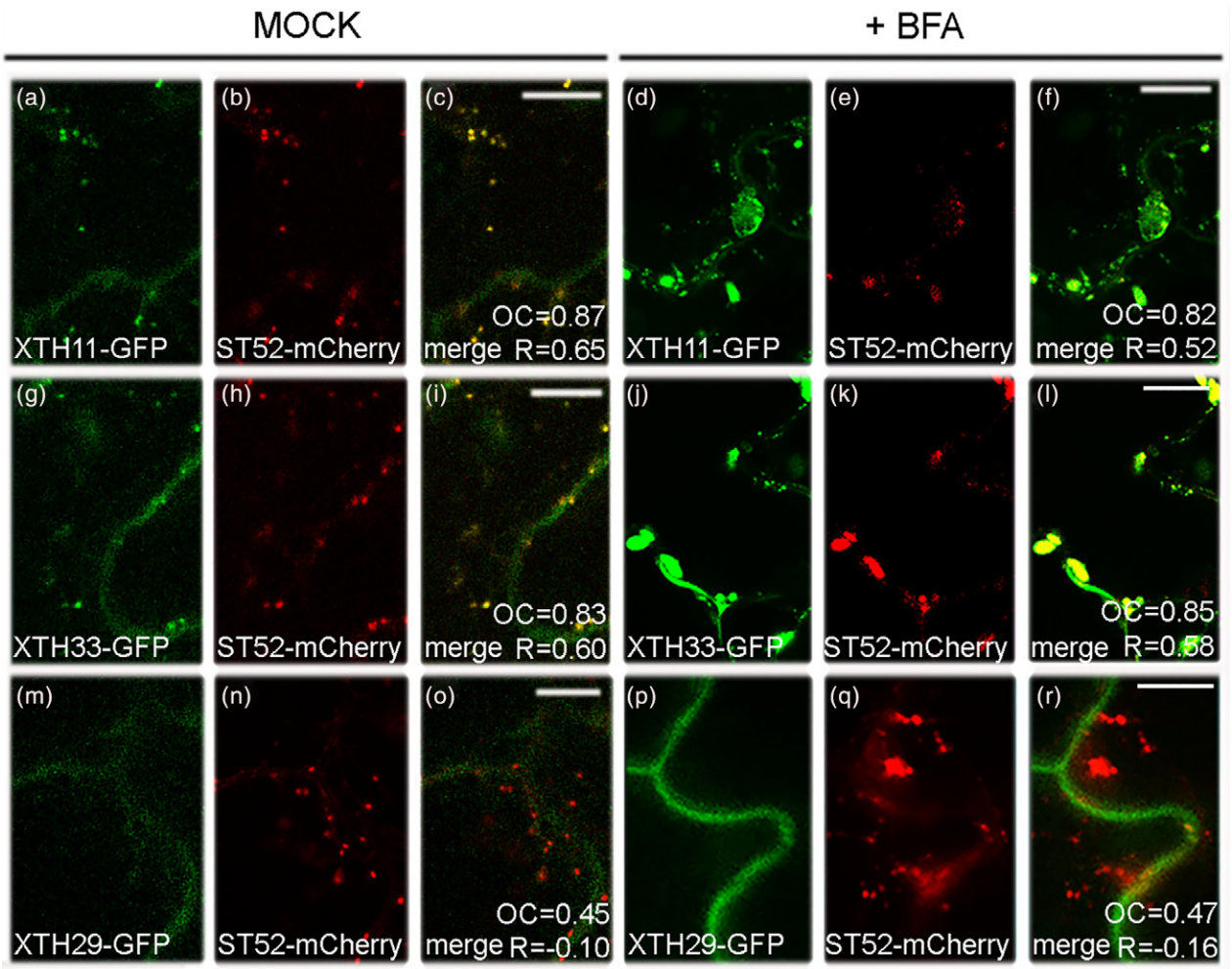

Figure 7. Effect of brefeldin A (BFA) on the secretion of the xyloglucan endotransglucosylase/hydrolases (XTHs) analyzed.
BFA (100 μM) affects the secretion pattern of XTH11-GFP (a–f), XTH33-GFP (g–l) and that of the colocalizing Golgi marker ST52-mCherry. BFA does not change the fluorescence distribution of XTH29-GFP (m, p), affecting the pattern of the co-expressed Golgi marker ST52-mCherry. Overlap coefficient (OC, after Manders) and *R* (Pearson's correlation coefficient) values are reported in each merged image. Statistical data are reported in Table S1. Scale bars: 5 μm.

DISCUSSION

Membrane trafficking is central to building up and remodeling the plant cell wall. Although matrix polysaccharides (pectins and hemicelluloses) are synthesized in the Golgi, but secreted proteins (structural and enzymatic) are cotranslationally translocated into the ER and modified afterwards in the Golgi, both components are assumed to reach the plasma membrane and, eventually, the cell wall through a conventional secretion pathway mediated by vesicles budding from the *trans*-Golgi network (Cosgrove, 2005; Kim and Brandizzi, 2014; 2016; Sinclair *et al.*, 2018). However, the large body of evidence for the existence of a UPS, as an alternative to the CPS and Golgi-independent transport, pushes for more targeted investigations into the mechanisms of protein delivery to the apoplast (Davis *et al.*, 2016; Ding *et al.*, 2014; Drakakaki and Dandekar, 2013; Robinson *et al.*, 2016; Wang *et al.*, 2017).

In this study, we provide clues that three members of the Arabidopsis family of XTHs, XTH11, XTH33 and XTH29, enzymes involved in the *in muro* remodeling of XGs, are secreted following different routes and molecular mechanisms. We also evidence a different involvement of the three XTHs in the cell response to drought and heat stress.

XTH11 and XTH33 reach their destination through a CPS pathway, whereas XTH29 undergoes a UPS route

Bioinformatic analyses predict that all *At*XTHs possess the N-terminus leader sequence required to enter the CPS pathway. XTH29 makes an exception and is hypothetically classified as LSP (SignalP 5.0 server). Thus, the secretion

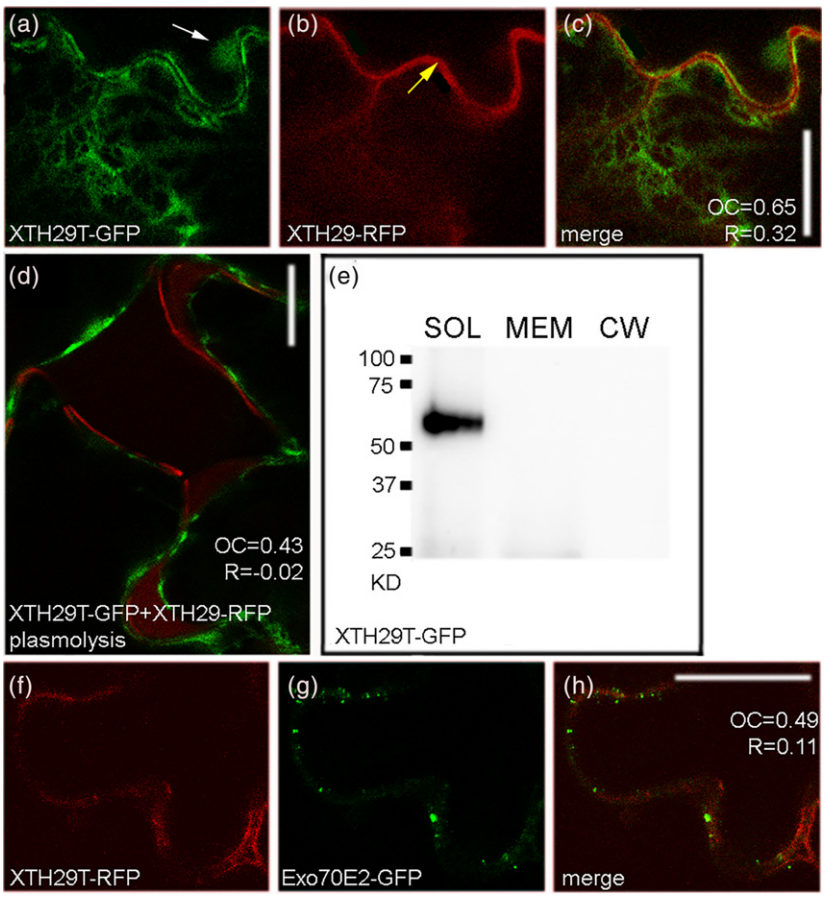

Figure 8. The truncated form of XTH29 neither reaches the cell wall nor is sequestered by EXPOs.
(a) Co-expression of XTH29T-GFP and XTH29-RFP shows the presence of XTH29T-GFP scattered in the cytoplasm and the nucleoplasm (white arrow) but not in the cell wall, which appears empty between two contiguous cells. (b–d) XTH29-RFP labels cell wall (yellow arrow, b) and does not colocalize with XTH29-GFP (c), as confirmed by plasmolysis test (d). (e) Western blot analysis shows XTH29T-GFP in the soluble protein fraction. (f–h) Co-expression of XTH29T-RFP and Exo70E2-GFP show no-localization of the two chimeras. (OC, after Manders) and *R* (Pearson's correlation coefficient) values are reported in each merged image. Statistical data are reported in Table S1. Scale bars: (a–c, f–h) 20 μm; (e) 5 μm.

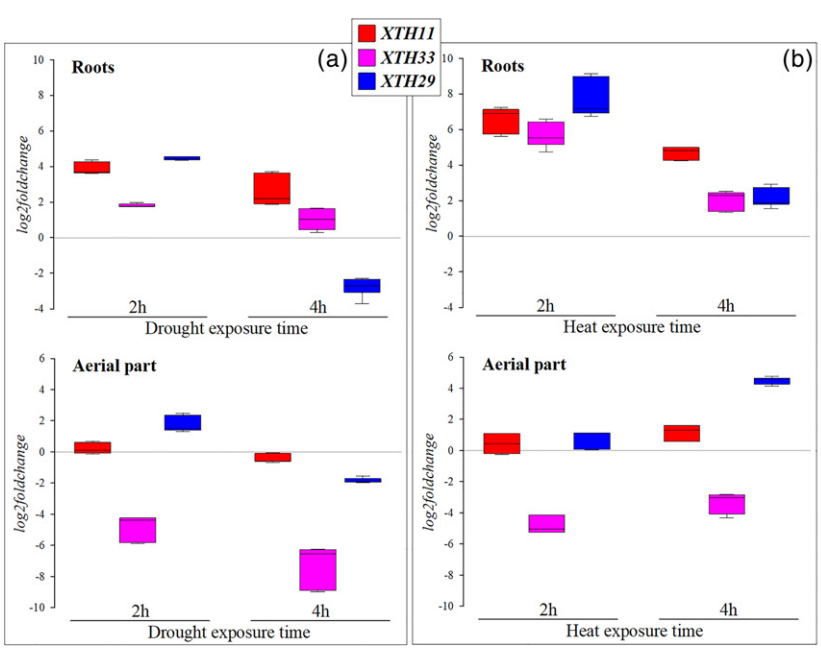

Figure 9. Expression pattern of *XTH11*, *XTH33* and *XTH29* in response to drought and heat stress.
Quantitative real-time polymerase chain reaction of XTH11, XTH33 and XTH29 in roots and aerial parts of a 4-week-old Arabidopsis seedlings subjected to drought (a) and heat (42°C) (b) stress for 2 and 4 h. The expression of *XTH* genes is reported as transcript inhibition level (log2 of fold change) with respect to time 0 (control). The results of three independent biological and three technical replicates are presented with box plots (middle bar, median; box limits, upper and lower quartiles; whiskers, min. and max. values).

pattern of XTH29 was compared with that of XTH11 and XTH33 by expressing the GFP-tagged forms of the three proteins in Arabidopsis cotyledons. Our results show that both XTH11-GFP and XTH33-GFP, passing through the Golgi stacks, undergo a CPS pathway, although it cannot be excluded that they may bypass the *trans*-Golgi network,

as recently reported (Elliot *et al.*, 2020). On the contrary, XTH29-GFP reaches the cell wall through a very different secretion pattern, labeling very small punctate structures that are distinct from the Golgi stacks.

The characteristics of XTH29, revealed by the predictive model and confocal microscopy observations, fully satisfies the attributes required for a protein to follow the UPS pathway indicated by Regente *et al.* (2012), as it lacks an SP, does not possess TM domains for ER and Golgi, bypasses the Golgi and is BFA insensitive. Several LSPs have been reported in plants, usually by secretome studies (Agrawal *et al.*, 2010). Most of them seem related to stress or pathogen infection responses, but some also appear to be involved in plant growth and development processes. The sunflower protein jacalin-related lectin (Helja) was the first extracellular LSP protein predicted to undergo a UPS (Pinedo *et al.*, 2012). Similarly, SAMS2, another LSP protein involved in lignin methylation, was proposed as a cargo of EXPO by immunoelectron microscopy observations and colocalization with the specific marker Exo70E2 (Wang *et al.*, 2010). Furthermore, three Arabidopsis galactosyltransferases (GALT14A, GALT29A and GALT31A), expressed in tobacco, were localized in the EXPOs, other than in the Golgi, suggesting a role of EXPO in the biosynthesis of arabinogalactans (Poulsen *et al.*, 2014). Exo70 is one of the eight protein subunits of the exocyst complex, evidenced in yeasts, mammals and plants (Hála *et al.*, 2008; Saeed *et al.*, 2019). In Arabidopsis, it has over 23 paralogs with possible specific and distinct roles during secretion (Zárský *et al.*, 2009; 2020). Exo70E2 has been specifically identified in vesicles involved in unconventional exocytosis (Wang *et al.*, 2010). EXPO, the double membranes of which are labeled by Exo70E2, was shown to fuse with the plasma membrane, releasing a single-membrane-bound vesicle containing SAMS2 as cargo (Wang *et al.*, 2010; 2017). In this article, we show that the fluorescent EXPO marker Exo70E2-GFP colocalizes with the XTH29-RFP-labeled punctate structures present in the cytosol, near the plasma membrane, and in the extracellular space between the plasmolyzed plasma membrane and the cell wall. On the contrary, the XTH29-labeled compartments were distinct from autophagosomes (tagged by Exo70B1). Therefore, EXPO could mediate XTH29 secretion through a UPS pathway. Doubts on the biological function of Exo70E2 have been raised, as its subcellular localization might be an artifact of the *35S* promoter-driven overexpression. Furthermore, some authors believe that Exo70E2 compartments are a form of autophagosome related to a specific subtype of autophagic process, the so-called secretory autophagy pathway, connected to UPS and involving exosome production (Zárský *et al.*, 2020). Undoubtedly, autophagosomes and EXPO are morphologically similar and, although their specific markers (ATG8 and Exo70E2, respectively) do not colocalize in physiological conditions, both accumulate in the vacuole upon autophagy induction, suggesting that they are somehow related (Lin *et al.*, 2015; Robinson *et al.*, 2016). Recently, evidence has been provided on the possible role of *At*NBR1-mediated selective autophagy for regulating exocyst homeostasis in plants. In contrast to the direct *At*Exo70B2–*At*ATG8 binding, an indirect *At*Exo70E2–*At*NBR1–*At*ATG8 interaction for the recruitment to autophagosomes has been hypothesized for *At*Exo70E2 recycling (Ji *et al.*, 2020). However, we have never found fluorescence linked to Exo70E2 or XTH29 in the vacuole, so that the problem of recycling Exo70E2 and/or EXPO involved in UPS trafficking to the cell wall remains an interesting point to be explored. Although, in our experimental system, XTH29-RFP and Exo70E2-GFP were overexpressed under the control of the *35S* promoter, the precise overlapping of their fluorescent secretion patterns towards the wall strongly suggests a strict relationship between the proteins. As reported for SAMS2, we propose that XTH29 is the cargo of EXPO (or secretory autophagosomes) that mediate the UPS of proteins with specific roles in the dynamic remodeling of the plant cell wall.

Some peculiar characteristics have been reported for EXPO formation and their protein cargo secretion pattern. Exo70E2 is known to play a specific and crucial role in EXPO formation in plants and animals; in fact, the overexpression of Exo70E2 induces EXPOs in plant and human embryonic kidney (HEK293A) cells (Ding *et al.*, 2014). Similarly, we observed a clear increase of the number of EXPOs when Exo70E2-GFP and XTH29-RFP were co-expressed. On the contrary, the fluorescent pattern described for SAMS2 seems, in some details, different from that of XTH29-GFP. In Arabidopsis protoplast observations, over 48 h was required to move from a general cytosolic distribution of SAMS2-GFP to a punctate pattern colocalizing with Exo70E2-mRFP (Wang *et al.*, 2010). In Arabidopsis cotyledon epidermal cells, XTH29-GFP showed, instead, a punctate pattern starting early in its expression and the punctae became more evident when Exo70E2 was co-expressed. In agreement, Poulsen *et al.* (2014) described no scattered cytoplasmic distribution for *At*GALT31A. These differences in the early pattern of EXPO protein cargo could depend on the experimental system used (i.e. protoplasts or epidermal tissues); however, it is very difficult to speculate on these aspects as the molecular mechanisms of protein recruitment by EXPOs are yet to be understood.

The multiple alignment analysis of XTH29 and SAMS2 showed a similarity of about 50% in the ETR of approximately 45 aa of XTH29, common to a restricted number of XTHs and located downstream of XET-C (Johansson *et al.*, 2004). The ETR 45-aa domain appears to play a determinant role in XTH29 apoplast targeting; in fact, its depletion prevented the truncated protein from reaching the final destination and being sequestrated by EXPOs.

Significantly, the fluorescent construct of the ETR fragment (RFP-45aaF) showed a typical cytosolic pattern, indicating that the isolated terminal XTH29 domain, although needed, has no sufficient information to address a protein to the wall or allow protein recruitment by EXPOs.

The subcellular localization of XTH11, XTH29 and XTH33 is different

Another important point that distinguishes the three XTHs is their final localization. According to Ndamukong *et al.* (2009), our results confirmed that XTH33 is associated with the plasma membrane, unlike XTH11 and XTH29 that stably localize in the cell wall. Similarly to XTH33, XTH17 and XTH31 are known to target the plasma membrane, where they might function as a dimer to modify the newly secreted XGs (Zhu *et al.*, 2012; 2014). XGs undergo transglycosylation immediately after cell wall release. Two different sets of XTHs operate integrational or restructuring processes involved in the *in muro* incorporation of newly synthesized XGs and in the reorganization of pre-existing wall-bound XGs, respectively (Thompson and Fry, 2001; Vissenberg *et al.*, 2000). The great number of *XTH* genes in plants and their diversified expression profiles hint at the distinct physiological roles of these proteins in cell wall dynamics (Becnel *et al.*, 2006). Plasma membrane-associated XTHs (i.e. XTH17, XTH31 and XTH33) are likely to function in integrational processes of newly secreted XGs, whereas cell wall XTHs (e.g. XTH11 and XTH29) are possibly involved in the remodeling of the cellulose/XG network.

To gain a deeper insight into the role of XTH33, we assessed its possible release into the wall. Confocal images of plasmolyzed Arabidopsis cotyledons clearly evidenced the presence of XTH33 in both the plasma membrane and the cell wall. This was confirmed by Western blot analyses, which also indicated the existence of a truncated form of XTH33 within the wall. By constructing two different XTH33 chimeras carrying GFP or RFP fused to the N- or C-termini, respectively, we found that, upon plasmolysis, the cell wall was exclusively marked by the red tag linked to the C-terminus, indicative of XTH33 cleavage. Comparing the aa sequence and the molecular weight of the XTH33 truncated form, the active catalytic motif was deduced to remain attached to the plasma membrane domain of the protein and not to the hydrolyzed C-terminus released in the cell wall. The XET-C domain of Angiosperm XTHs is characterized by the presence of four cysteine residues supposed to enhance protein stability through the formation of disulfide bridges. It also seems to have a role in the recognition and guidance of XG substrates to the active site (Johansson *et al.*, 2004). This motif is strongly conserved during plant evolution, also being present in *Selaginella* XTH1, where disulfide bond reduction was demonstrated to reduce the activity of XET (Van Sandt *et al.*, 2006). The XTH33 fragment released in the cell wall includes the XET-C domain and the cysteine residues (Figure S4); thus, its elimination may represent a post-transcriptional mechanism to change protein affinity for XGs and control XET activity. Significantly, the plausible distribution of XTH33 at discrete areas of the plasma membrane, probably in correspondence with particular cell wall domains and under the control of specific cleavage enzymes, is an attractive hypothesis that deserves further investigation. It is worth noting that the truncated form of XTH33 was also detected in Arabidopsis cotyledons transformed with the native form of the protein, indicating that cleavage is not related to an aberrant recombinant protein. Furthermore, when tested for functionality, all native and GFP-tagged XTHs analyzed showed XET activity (Figure S8).

***XTH11, XTH29* and *XTH33* are differentially expressed in heat and drought stress responses**

Quantitative real-time polymerase chain reaction (RT-qPCR) analyses revealed different gene transcription levels for the three XTHs in the root and aerial parts of Arabidopsis seedlings, and in response to heat and drought stresses. Despite that a low correlation between transcriptome and proteome is widely recognized, the different secretion pathways followed by the XTHs analyzed could be related to a differential involvement of the three proteins in cell wall remodeling in response to stress. Nevertheless, further integrated investigations are required to confirm this assumption. In the root, heat stress caused a high and immediate increase in the expression of all three *XTH* genes, especially after the initial 2 h of treatment. This increase was very relevant for *XTH29* reported to be expressed at very low levels in Arabidopsis plants (Yokoyama and Nishitani, 2001a). Several studies demonstrated that the root is more sensitive to heat stress than are the other plant organs (Janni *et al.*, 2020; Le Gall *et al.*, 2015; Liu and Huang, 2005). Therefore, an overexpression of all three *XTH* genes in the root could be related to their involvement in a rapid heat stress response, which subsequently affects the whole plant. An increased expression of *XTH*s seems required to promote cell wall strengthening by increasing XG lengths and helping plants to adapt to high temperatures by reinforcing the connections between primary and secondary walls (Baumann *et al.*, 2007; Iurlaro *et al.*, 2016; Yang *et al.*, 2006). In the root, drought stress affected the expression of only *XTH11* and *XTH29* isoforms with, once again, a significant over-regulation of *XTH29* in the first 2 h of treatment, which might, thus, play a specific role in the response to stress in this organ. In the aerial part of seedlings, *XTH29* was overexpressed after 4 h of heat stress, whereas *XTH33* was strongly downregulated by both heat and drought stress, with responses similar to those reported for *XTH6*, *XTH9*, *XTH15* and *XTH16* (Clauw *et al.*, 2015).

In physiological conditions, *XTH11* was reported to be mainly expressed in the roots (Yokoyama and Nishitani, 2001a). We found that, in the same organ, *XTH11* expression was differentially upregulated by heat and drought stress. Heat stress also induced a root-specific overexpression of *XTH33*, although in Arabidopsis it was found to be predominantly expressed in the green siliques (Yokoyama and Nishitani, 2001a). XTH33 is one of the few proteins of the XTH family localized at discrete domains of the plasma membrane and is hypothesized to act in the modification and integration of newly secreted XGs, as discussed above. If this hypothesis is correct, the integration of newly synthesized XGs into the wall may represent a root-specific response to heat stress. Although *XTH29* expression is very limited in all Arabidopsis organs (Yokoyama and Nishitani, 2001a), our results showed a differential overexpression of the gene, depending on organ and stress typology, with the exception of the aerial parts subjected to drought stress, where no significant fold change was recorded. Thus, XTH29 may play a role in response to severe stress, as is assumed for most LSPs undergoing a UPS pathway (Davis *et al.*, 2016; Ding *et al.*, 2014; Robinson *et al.*, 2016; Wang *et al.*, 2017). It is plausible that the XTH29 UPS prompts a higher stress response than XTH11 and XTH33 CPS, taking part in specific and diversified rearrangements of the cellulose/XG network. Accordingly, different roles in persimmon fruit cell wall modifications have been proposed for *DkXTH6* and *DkXTH7*, showing diversified and opposite expression levels in mature and growing tissues. Significantly, the proteins differ in having an SP or not (Han *et al.*, 2016a). The secretion patterns of the two *Dk*XTHs were not analyzed; therefore, we can only suppose that the absence of the SP is indicative of a UPS for *Dk*XTH7. Similar to our results on XTHs, the different transport mechanisms of *Dk*XTHs are likely related to the action specificity of the proteins in the cell wall. In fact, the opposing expression patterns of the proteins suggest that DkXTH6 takes part in cell wall restructuring and that DkXTH7 is involved in cell wall assembly, indicating their special roles in persimmon fruit softening (Han *et al.*, 2016a).

In summary (Figure 10), comparing the secretion patterns of three XTH family members involved in the *in muro* remodeling of the XG network, we showed that XTH11 and XTH33 reach their site of action (the cell wall and the plasma membrane, respectively) through a conventional secretion pathway; on the contrary, XTH29, a predicted LSP, undergoes an unconventional route involving EXPOs. Our knowledge of the molecular mechanisms controlling unconventional secretion remains poor: the results obtained on the role of the last 45-aa domain of XTH29, which is necessary but not sufficient for cell wall targeting through EXPO, may help future investigations characterize the unconventional secretion of XTH29. The assumption that plants respond to stress by the secretion of a high number of LSPs resulted from a proteomic approach (Agrawal *et al.*, 2010; Ding *et al.*, 2014). In this article, we provide evidence that *XTH29*, known to be poorly expressed in physiological conditions (Yokoyama and Nishitani, 2001a), is significantly upregulated by drought and thermal stress, evidencing a possible role for UPS-secreted XTH29 as reported for most LSPs undergoing unconventional secretion (Wang *et al.*, 2017).

EXPERIMENTAL PROCEDURES

Plasmid construction

Arabidopsis *XTH11* (AT3G48580), *XTH29* (AT4G18990) and *XTH33* (AT1G10550) were purchased from The Arabidopsis Information Resource (TAIR, https://www.arabidopsis.org). The cDNAs (50 ng) were amplified by PCR to introduce *Bam*HI and *Nhe*I restriction sites in each gene, using the primers reported in Table S3. The *Bam*HI/*Nhe*I fragments were introduced into

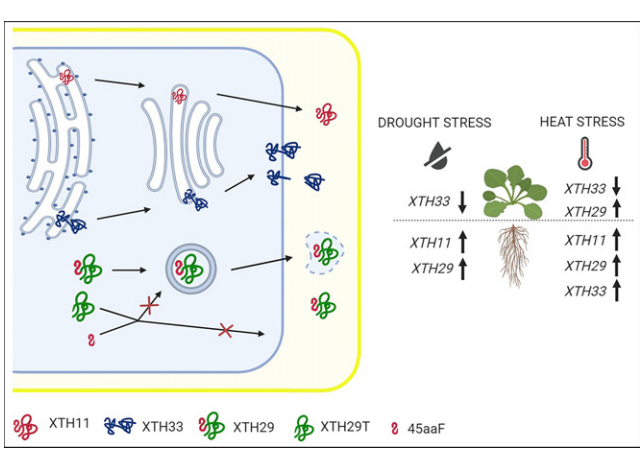

Figure 10. Schematic representation of Arabidopsis XTH11, XTH33 and XTH29 showing different secretory routes and their involvement in stress responses.

GFP/RFP-containing vectors (De Caroli *et al.*, 2015) to obtain the constructs listed in Figure S1. *XTH33* was also amplified to introduce *Sal*I and *Pst*I restriction sites and the obtained fragment was introduced into the secGFP-PMEI1 vector, where sec is an Arabidopsis chitinase ER SP (De Caroli *et al.*, 2011b). The construct secGFP-XTH33 was obtained. To obtain XTH29T-GFP/RFP, the *Nhe*I restriction site was inserted before the coding region for 45aaF and the resultant *Bam*HI/*Nhe*I fragment was introduced into a GFP-containing vector (De Caroli *et al.*, 2015). The coding region for 45aaF was amplified, introducing *Sal*I and *Sac*I restriction sites, and cloned in the RFP-Rab11 construct (Rehman *et al.*, 2008). All constructs were checked by sequencing (Eurofins Genomics, https://www.eurofinsgenomics.eu). All constructs were inserted as *Bam*HI/*Kpn*I fragments in the plant binary vector (Haseloff *et al.*, 1997) with CaMV *35S*-driven expression. *Agrobacterium tumefaciens* (strain LBA4404) was used for transient gene expression and in Arabidopsis seedling cotyledons using the Fast Agro-mediated Seedling Transformation (FAST) method (Li *et al.*, 2009).

Plant growth for co-cultivation and stress treatments

For co-cultivation experiments, *A. thaliana* (Col-0) seedlings were grown as previously reported (Lionetti *et al.*, 2017). Arabidopsis (Col-0) seeds (approx. 30 per experiment), vernalized at 4°C in the dark for 24 h, were germinated on modified Murashige and Skoog (MS, 1.1 g L^{-1} salts, 10 g L^{-1} sucrose, 8 g L^{-1} agar) and grown for 5–6 days. They were soaked in the same Petri dish with 10 ml of co-cultivation medium (modified MS without agar, 0.1 mM acetosyringone, 0.005% Silwet L-77) supplemented with exponentially grown *Agrobacterium tumefaciens* cells at a final density of OD_{600} = 0.5, equivalent to 6 × 10^8 colony forming units (cfu) ml^{-1}. Co-cultivation was carried out in darkness at the same temperature as seedling growth for 48–72 h before microscopic observations. For cotransformation experiments, an equal amount of two transformed *Agrobacterium* was added at a final density of OD_{600} = 0.5 (6 × 10^8 cfu ml^{-1}).

For heat and drought stress treatments, sterile *A. thaliana* seeds (10 per experiment), vernalized at 4°C in the dark for 24 h, were placed vertically on square Petri dishes (120 × 120 mm) containing modified MS (2.2 g L^{-1} salts, 1% sucrose, 1% agar) at 21°C, with a cycle of 16 h of light (100 μE) at 22°C followed by 8 h of dark at 18°C. For dehydration experiments, 4-week-old seedlings were carefully transferred to new Petri dishes containing a well water-moistened (control) or dry (stressed) Whatman No. 1 filter paper for 2 and 4 h, at 21°C, in the dark. Heat stress treatment was induced on the 4-week-old seedlings incubated at 22°C (control) and 42°C (stressed) in the dark for 2 and 4 h. In both dehydration and thermal experiments, the condition of darkness was preferred to avoid any possible interference between light and stress responses. At the end of the incubation period, root and aerial parts of the seedlings were excised from control and stressed seedlings, immediately surface-dried on Whatman No. 1 filter paper, weighed and then frozen in liquid nitrogen.

For BFA (Sigma-Aldrich, http://www.sigmaaldrich.com) treatment, transformed Arabidopsis seedlings were treated by immersion in a solution of BFA (dissolved in DMSO) at the final concentration of 100 μM, as reported by De Caroli *et al.* (2020). Control tests were carried out under normal conditions (mock treatments) and with DMSO.

Plasmolysis was induced by the incubation of seedling in 1 M NaCl hypertonic solution for 10 min.

Enzyme extraction, preparation of XXXGol-sulforhodamine conjugate (XXXGol-SR) and biochemical assay of extracted XET activity

XTH11, XTH29, XTH33, XTH11-GFP, XTH29-GFP, XTH33-GFP secGFP-XTH33 and wild-type (WT) cotyledons were processed for enzyme extraction, as reported by Fry *et al.* (2008). Samples were homogenized by a Potter–Elvehjem glass homogenizer in 20 volumes (w/v) of ice-cold extraction buffer (10 mM $CaCl_2$, 300 mM succinate (Na^+, pH 5.5), 20 mM ascorbate, 15% v/v glycerol and 3% w/v polyvinylpolypyrrolidone) and extracted for 2 h at 4°C with constant shaking. The extracts were filtered on Miracloth® (EMD Millipore, now Merck, https://www.merckmillipore.com) and centrifuged at 12 000 ***g*** for 5 min. The supernatants (crude enzyme extracts) were stored in single-use aliquots at −80°C.

The xyloglucan heptasaccharide XXXG (10.62 mg; 10 mmol) from Megazyme (https://www.megazyme.com) was reductively aminated to convert the reducing terminal glucose moiety to 1-amino-1-deoxyglucitol, and then fluorescently labeled by the reaction of the amino group with lissamine rhodamine sulfonyl chloride to form a stable sulphonamide conjugate (XXXGol-SR), according to the method described by Fry (1997).

A reaction mixture formed by mixing each crude XTH extract (10 μl), 1% tamarind XG solution (5 μl) and 6 mM XXXGol-SR (5 μl) was incubated for 18 h in the dark at room temperature (22°C). Control samples were prepared adding the extraction buffer instead of the crude XTH extracts to the mixture. After incubation, 5 μl of the reaction mixture was dried on a Whatman filter paper No. 3 (Whatman, now Cytiva, https://www.cytivalifesciences.com). To de-stain the background, the paper was washed under tap water for 16 h. The dried paper was examined under an ultraviolet lamp (λ = 254 nm). The XET activity of the extracted XTH is indicated by a pale pink spot emitting an intense orange fluorescence. Images were acquired with a digital camera (Coolpix 8800; Nikon, https://www.nikon.com) in a dark room at the highest resolution (8.0 Megapixel). The emitted fluorescence was quantified with IMAGEJ (National Institutes of Health, https://imagej.nih.gov/ij/) as absolute pixel intensity. After subtracting the average non-specific fluorescence of controls from all samples, variations in XET activity were expressed as pixel intensity percentage relative to weight sample, the average intensity of which was arbitrarily assigned an XET activity value of 100%.

Confocal laser scanning microscopy

Transiently transformed Arabidopsis cotyledons were observed by a confocal laser scanning microscope (LSM 710; Zeiss, http://www.zeiss.com). Observations were performed as described in De Caroli *et al.* (2014). The distribution of each fluorescent protein was observed in $3 < n < 5$ independent transformation experiments. The confocal images were acquired at different scanning depths (Figure S13) and the most representative among them were chosen and processed using PHOTOSHOP 7.0 (Adobe, https://www.adobe.com). The evaluation of the EXPO number was carried out counting the intracellular compartments in 12 confocal sections of equivalent areas acquired by the same transformed cotyledon. This counting was performed for three independent experiments. The results are presented as the mean values ± standard deviations.

For quantitative colocalization analyses, the overlap coefficient (OC, after Manders) and the Pearson's correlation coefficient (*R*) were evaluated on 15 confocal images using the Zeiss LSM 710

software (CO-LOCALIZATION VIEW) and reported for each merged image. OC indicates an actual overlap of the signals and represents the true degree of colocalization, with values ranging from 0 to +1; *R* provides information about the similarity in shape between the two patterns, with a value range of −1 to +1 (Zinchuk *et al.*, 2007).

Protein extraction, phase separation and immunoblotting analyses

Transformed cotyledons were crushed in a pre-cooled Eppendorf™ Micropestle (ThermoFisher Scientific, https://www.thermofisher.com) with liquid nitrogen until a fine powder was obtained. The powder was suspended in homogenization buffer (40 mM Hepes-NaOH buffer, pH 7.5, 10 mM imidazole, 1 mM benzamidine, 5 mM 6-aminohexanoic acid, 10 mM dithiothreitol and 1 mM phenylmethylsulfonyl fluoride). The homogenate was centrifuged at 800 ***g*** for 10 min at 4°C. The resulting pellet, consisting of cell walls and cell debris, was sequentially treated with 1 ml of homogenization buffer (three times), 1 ml of chloroform/methanol (1/1 v/v; 10 times) and acetone (three times). De-lipidated cell walls were suspended in phenol:acetic acid:water (2:1:1 w/v/v) and stirred twice for 20 min each at 70°C. After centrifugation (8700 ***g***, 10 min) the extracted non-covalently bound cell wall (CW) proteins present in the supernatant were precipitated with 0.1 M ammonium acetate in methanol overnight (Lenucci *et al.*, 2006). The supernatant, representing the protein intracellular fraction, including endomembrane compartments and organelles, was precipitated with 80% acetone at −20°C overnight and centrifuged at 10 000 ***g*** for 10 min at 4°C. The resulting pellet was suspended in 1.5 ml of TBS (10 mM Tris-buffer, pH 7.5, 0.15 M NaCl, 1 mM EDTA) containing 2% (v/v) Triton X-114 and partitioned into detergent and aqueous phases by temperature-induced phase separation (32°C) for 3 min and, successively, centrifuged at 10 000 ***g*** for 20 s. The aqueous phase, enriched with soluble (SOL) proteins, was collected and precipitated with 80% acetone at −20°C overnight. The detergent phase, enriched with membrane (MEM)-bound proteins, was re-extracted three times with 1.5 ml of TBS containing 0.06% Triton-X114 (De Caroli *et al.*, 2011b). Protein concentration was determined as described by Bradford (1976). An identical quantity of SOL, MEM and CW protein fractions (10 μg per line) was subjected to SDS-PAGE and Western blotting. Anti-GFP (1:5000 v/v) (Molecular Probes, now ThermoFisher Scientific, https://www.thermofisher.com) and anti-XTH (Agrisera, https://www.agrisera.com) were used in TBS +1% skimmed-milk powder. All primary antibodies were combined with anti-rabbit secondary antibodies coupled to peroxidase (1:10 000 v/v) (Sigma-Aldrich). Protein bands were enhanced with the ECL™ Western Blotting Analysis System (GE Healthcare, http://www.gehealthcare.com) and their molecular weight was measured using an image analyzer (EDAS 290; Kodak, https://www.kodak.com) and the software 1D 3.6. Each experiment was independently repeated three times for each fusion protein.

Standard RNA procedures and RT-qPCR

Total RNA was isolated from the roots and aerial parts of 4-week-old seedlings subjected or not to different stresses for 0 (control), 2 and 4 h, as previously reported (Iurlaro *et al.*, 2016). RT-qPCR analysis was performed using SYBR Green fluorescent detection in a CFX96 Real-Time System Cycler (Bio-Rad, https://www.bio-rad.com) with three biological and three technical replicates per sample. The primer sequences used are reported in Table S4. The PCR program was as follows: 10 min at 95°C; 50 cycles of 15 s at 95°C, 20 s at 60°C and an increment of 0.5°C every 0.5 s from 65°C to 95°C. The specificity of PCR products was checked in a melting-curve test. The Arabidopsis *actin 2* (*act2*, AT3G18780), *actin8* (*act8*, AT1G49240) and *EF1α* (AT1G18070) genes are tested as reference genes. All genes under stress conditions and during 0–4 h had a variation coefficient below 0.1, which is described as negligible variation under stress conditions in Arabidopsis, according to Czechowski *et al.* (2005). The *EF1α* gene was chosen as the reference gene because it showed the lowest variation coefficient among the genes (Table S5). Differences in gene expression between treated and untreated samples were considered significant when the expression was at least doubled (greater than or equal to twofold upregulation) or halved (less than or equal to twofold downregulation), according to Chen *et al.* (2007).

ACKNOWLEDGEMENTS

The authors would like to thank Prof. Liwen Jiang for kindly providing Exo70E2-GFP cDNA. We give special thanks to the 'Regione Puglia' for supporting the Project No. 14 'Reti di Laboratori Pubblici di Ricerca' 'SELGE', through which a Zeiss LSM710 confocal microscope was bought.

AUTHOR CONTRIBUTIONS

MDC, MSL and GP conceived the research and designed the experiments. MDC and EM performed the experiments. GP supervised the project, and MDC, EM, MSL and GP wrote the article. All of the authors read and approved the final version for publication.

CONFLICT OF INTEREST

The authors declare that they have no conflicts of interest associated with this work.

DATA AVAILABILITY STATEMENT

All relevant data supporting the results presented in this work are available within the article and the supporting materials.

SUPPORTING INFORMATION

Additional Supporting Information may be found in the online version of this article.

Figure S1. Schematic representation of the fusion proteins analyzed in this study.

Figure S2. *Arabidopsis* cotyledon epidermal cells co-expressing the analyzed fusion proteins and the plasma membrane marker pm-rk under control conditions (mock treatments).

Figure S3. Western blot of xyloglucan endotransglucosylase/hydrolase (XTH)11, XTH33 and XTH29.

Figure S4. Predicted hydrolysis site of XTH33.

Figure S5. Fluorescence distribution of XTH29-RFP.

Figure S6. Co-expression of XTH29-RFP and Exo70B1-GFP.

Figure S7. Co-expression of XTH11-RFP or XTH33-RFP with Exo70E2-GFP.

Figure S8. Xyloglucan endotransglucosylase (XET) activity in wild-type and transformed *Arabidopsis* cotyledons.

Figure S9. *Arabidopsis* cotyledon epidermal cells co-expressing the analyzed fusion proteins and the ST52-mCherry Golgi marker in control conditions (mock treatments) and in presence of DMSO (1% v/v).

Figure S10. Extra-terminal region (ETR) of XTH29.

Figure S11. The truncated form of XTH29 does not colocalize with the endoplasmic reticulum (ER) and Golgi markers.

Figure S12. Fluorescence distribution of RFP-45aaF.

Figure S13. *Z*-stack images of entire cells expressing XTH11-GFP.

Table S1. Mean ± standard deviation of the overlap coefficient (OC, after Manders) and the Pearson's correlation coefficient (*R*) of the reported merged images, evaluated on 15 confocal acquisitions.

Table S2. Amplification output values are expressed as $2^{-\Delta Cq} \pm SD$ for XTH11, XTH33 and XTH29 mRNAs (in control condition and after drought and heat stress), and are considered as proportional to the amount of mRNA target according to Schmittgen and Livak (2008).

Table S3. Primers for plasmid construction.

Table S4. Primers for gene expression analysis.

Table S5. Tested reference genes.

REFERENCES

Agrawal, G.K., Jwa, N.S., Lebrun, M.H., Job, D. & Rakwal, R. (2010) Plant secretome: unlocking secrets of the secreted proteins. *Proteomics*, **10**, 799–827.

Baumann, M.J., Eklöf, J.M., Michel, G., Kallas, A.M., Teeri, T.T., Czjzek, M. *et al.* (2007) Structural evidence for the evolution of xyloglucanase activity from xyloglucan endo-transglycosylases: Biological implications for cell wall metabolism. *The Plant Cell*, **19**, 1947–1963.

Becnel, J., Natarajan, M., Kipp, A. & Braam, J. (2006) Developmental expression patterns of Arabidopsis XTH genes reported by transgenes and genevestigator. *Plant Molecular Biology*, **61**, 451–467.

Bradford, M.M. (1976) A rapid and sensitive method for the quantitation of microgram quantities of protein utilizing the principle of protein-dye binding. *Analytical Biochemistry*, **72**, 248–254.

Chen, J.J., Wang, S.J., Tsai, C.A. & Lin, C.J. (2007) Selection of differentially expressed genes in microarray data analysis. *Pharmacogenomics Journal*, **7**, 212–220.

Clauw, P., Coppens, F., De Beuf, K., Dhondt, S., Van Daele, T., Maleux, K. *et al.* (2015) Leaf responses to mild drought stress in natural variants of *Arabidopsis*. *Plant Physiology*, **167**, 800–816.

Cosgrove, D.J. (2001) Plant cell walls: wall-associated kinases and cell expansion. *Current Biology*, **11**, 558–559.

Cosgrove, D.J. (2005) Growth of the plant cell wall. *Nature Reviews Molecular Cell Biology*, **6**, 850–861.

Cosgrove, D.J. (2018) Nanoscale structure, mechanics and growth of epidermal cell walls. *Current Opinion in Plant Biology*, **46**, 77–86.

Czechowski, T., Stitt, M., Altmann, T., Udvardi, M.K. & Scheible, W. (2005) Genome-wide identification and testing of superior reference genes for transcript normalization in *Arabidopsis*. *Plant Physiology*, **139**, 5–17.

Davis, D.J., Kang, B.H., Heringer, A.S., Wilkop, T.E. & Drakakaki, G. (2016) Unconventional protein secretion in plants. In: Pompa, A. & De Marchis, F. (Eds.) *Methods in molecular biology*. Humana Press, 1459, pp. 47–63.

De Caroli, M., Lenucci, M.S., Di Sansebastiano, G.P., Dalessandro, G., De Lorenzo, G. & Piro, G. (2011a) Dynamic protein trafficking to the cell wall. *Plant Signaling and Behavior*, **6**, 1012–1015.

De Caroli, M., Lenucci, M.S., Di Sansebastiano, G.P., Dalessandro, G., De Lorenzo, G. & Piro, G. (2011b) Protein trafficking to the cell wall occurs through mechanisms distinguishable from default sorting in tobacco. *The Plant Journal*, **65**, 295–308.

De Caroli, M., Lenucci, M.S., Di Sansebastiano, G.P., Tunno, M., Montefusco, A., Dalessandro, G. *et al.* (2014) Cellular localization and biochemical characterization of a chimeric fluorescent protein fusion of Arabidopsis cellulose synthase-Like A2 inserted into Golgi membrane. *The Scientific World Journal*, **2014**, 792420.

De Caroli, M., Lenucci, M.S., Manualdi, F., Dalessandro, G., De Lorenzo, G. & Piro, G. (2015) Molecular dissection of *Phaseolus vulgaris* polygalacturonase-inhibiting protein 2 reveals the presence of hold/release domains affecting protein trafficking toward the cell wall. *Frontiers in Plant Science*, **6**, 660.

De Caroli, M., Manno, E., Perrotta, C., De Lorenzo, G., Di Sansebastiano, G.P. & Piro, G. (2020) CesA6 and PGIP2 endocytosis involves different subpopulations of TGN-related endosomes. *Frontiers in Plant Science*, **11**, 350.

Ding, Y., Robinson, D.G. & Jiang, L. (2014) Unconventional protein secretion (UPS) pathways in plants. *Current Opinion in Cell Biology*, **29**, 107–115.

Drakakaki, G. & Dandekar, A. (2013) Protein secretion: how many secretory routes does a plant cell have? *Plant Science*, **203–204**, 74–78.

Eklöf, J.M. & Brumer, H. (2010) The XTH gene family: an update on enzyme structure, function, and phylogeny in xyloglucan remodeling. *Plant Physiology*, **153**, 456–466.

Elliot, L., Moore, I. & Kirchhelle, C. (2020) Spatio-temporal control of post-Golgi exocytic trafficking in plants. *Journal of Cell Science*, **133**, jcs237065.

Fry, S.C. (1989) The structure and functions of xyloglucan. *Journal of Experimental Botany*, **40**, 1–11.

Fry, S.C. (1997) Novel 'dot-blot' assays for glycosyltransferases and glycosylhydrolases: Optimization for xyloglucan endotransglycosylase (XET) activity. *The Plant Journal*, **11**, 1141–1150.

Fry, S.C. (2004) Primary cell wall metabolism: tracking the careers of wall polymers in living plant cells. *New Phytologist*, **161**, 641–675.

Fry, S.C., Mohler, K.E., Nesselrode, B.H. & Franková, L. (2008) Mixed-linkage beta-glucan: Xyloglucan endotransglucosylase, a novel wall-remodelling enzyme from *Equisetum* (horsetails) and charophytic algae. *The Plant Journal*, **55**, 240–252.

Genovesi, V., Fornalé, S., Fry, S.C., Ruel, K., Ferrer, P., Encina, A. *et al.* (2008) ZmXTH1, a new xyloglucan endotransglucosylase/hydrolase in maize, affects cell wall structure and composition in *Arabidopsis thaliana*. *Journal of Experimental Botany*, **59**, 875–889.

Gibeaut, D.M., Pauly, M., Bacic, A. & Fincher, G.B. (2005) Changes in cell wall polysaccharides in developing barley (*Hordeum vulgare*) coleoptiles. *Planta*, **221**, 729–738.

Hála, M., Cole, R., Synek, L., Drdová, E., Pecenková, T., Nordheim, A. *et al.* (2008) An exocyst complex functions in plant cell growth in Arabidopsis and tobacco. *The Plant Cell*, **20**, 1330–1345.

Han, Y., Ban, Q., Hou, Y., Meng, K., Suo, J. & Rao, J. (2016a) Isolation and characterization of two persimmon xyloglucan endotransglycosylase/hydrolase (XTH) genes that have divergent functions in cell wall modification and fruit postharvest softening. *Frontiers in Plant Science*, **7**, 624.

Han, Y.E., Ban, Q., Li, H., Hou, Y., Jin, M., Han, S. *et al.* (2016b) DkXTH8, a novel xyloglucan endotransglucosylase/hydrolase in persimmon, alters cell wall structure and promotes leaf senescence and fruit postharvest softening. *Scientific Reports*, **6**, 39155.

Han, Y., Wang, W., Sun, J., Ding, M., Zhao, R., Deng, S. *et al.* (2013) Populus euphratica XTH overexpression enhances salinity tolerance by the development of leaf succulence in transgenic tobacco plants. *Journal of Experimental Botany*, **64**, 4225–4238.

Han, Y.e., Zhu, Q., Zhang, Z., Meng, K., Hou, Y., Ban, Q. *et al.* (2015) Analysis of xyloglucan endotransglycosylase/hydrolase (XTH) genes and diverse roles of isoenzymes during persimmon fruit development and postharvest softening. *PLoS One*, **10**, e0123668.

Haseloff, J., Siemering, K.R., Prasher, D.C. & Hodge, S. (1997) Removal of a cryptic intron and subcellular localization of green fluorescent protein are required to mark transgenic Arabidopsis plants brightly. *Proceedings of the National Academy of Sciences of the United States of America*, **94**, 2122–2127.

Hayashi, T. (1989) Xyloglucans in the primary-cell wall. *Annual Review of Plant Physiology and Plant Molecular Biology*, **40**, 139–168.

Herburger, K., Franková, L., Pičmanová, M., Loh, J.W., Valenzuela-Ortega, M., Meulewaeter, F. *et al.* (2020) Hetero-trans-β-glucanase produces cellulose–xyloglucan covalent bonds in the cell walls of structural plant tissues and is stimulated by expansin. *Molecular Plant*, **13**, 1047–1062.

Hrmova, M., Farkas, V., Lahnstein, J. & Fincher, G.B. (2007) A barley xyloglucan xyloglucosyl transferase covalently links xyloglucan, cellulosic substrates, and (1,3;1,4)-beta-D-glucans [published correction appears in J Biol Chem. 2008 Oct 3;283(40):27344]. *Journal of Biological Chemistry*, **282**, 12951–12962.

Iurlaro, A., De Caroli, M., Sabella, E., De Pascali, M., Rampino, P., De Bellis, L. *et al.* (2016) Drought and heat differentially affect XTH expression and

XET activity and action in 3-day-old seedlings of durum wheat cultivars with different stress susceptibility. *Frontiers in Plant Science*, **7**, 1686.

Janni, M., Gullì, M., Maestri, E., Marmiroli, M., Valliyodan, B., Nguyen, H.T. *et al.* (2020) Molecular and genetic bases of heat stress responses in crop plants and breeding for increased resilience and productivity. *Journal of Experimental Botany*, **71**, 3780–3802.

Ji, C.-Y., Zhou, J., Guo, R., Lin, Y., Kung, C.-H., Hu, S. *et al.* (2020) AtNBR1 mediates selective autophagy of AtExo70E2 in Arabidopsis. *Plant Physiology*, **184**, 777–791.

Johansson, P., Brumer, H., Baumann, M.J., Kallas, Å.M., Henriksson, H., Denman, S.E. *et al.* (2004) Crystal structures of a poplar xyloglucan endotransglycosylase reveal details of transglycosylation acceptor binding. *The Plant Cell*, **16**, 874–886.

Kim, S.J. & Brandizzi, F. (2014) The plant secretory pathway: an essential factory for building the plant cell wall. *Plant Cell Physiology*, **55**, 687–693.

Kim, S.J. & Brandizzi, F. (2016) The plant secretory pathway for the trafficking of cell wall polysaccharides and glycoproteins. *Glycobiology*, **26**, 940–949.

Kulich, I., Pečenková, T., Sekereš, J., Smetana, O., Fendrych, M., Foissner, I. *et al.* (2013) Arabidopsis exocyst subcomplex containing subunit EXO70B1 is involved in autophagy-related transport to the vacuole. *Traffic*, **14**, 1155–1165.

Le Gall, H., Philippe, F., Domon, J.-M., Gillet, F., Pelloux, J. & Rayon, C. (2015) Cell wall metabolism in response to abiotic stress. *Plants*, **4**, 112–166.

Lenucci, M., Leucci, M.R., Andreoli, C., Dalessandro, G. & Piro, G. (2006) Biosynthesis and characterization of glycoproteins in *Koliella antarctica* (Klebsormidiales, Chlorophyta). *European Journal of Phycology*, **41**, 213–222.

Li, J.F., Park, E., von Arnim, A.G. & Nebenführ, A. (2009) The FAST technique: a simplified Agrobacterium-based transformation method for transient gene expression analysis in seedlings of Arabidopsis and other plant species. *Plant Methods*, **5**, 6.

Lin, Y., Ding, Y., Wang, J., Shen, J., Kung, C.H., Zhuang, X. *et al.* (2015) Exocyst-positive organelles and autophagosomes are distinct organelles in plants. *Plant Physiology*, **169**, 1917–1932.

Lionetti, V., Fabri, E., De Caroli, M., Hansen, A.R., Willats, W.G., Piro, G. *et al.* (2017) Three pectin methylesterase inhibitors protect cell wall integrity for Arabidopsis immunity to *Botrytis*. *Plant Physiology*, **173**, 1844–1863.

Liu, X. & Huang, B. (2005) Root physiological factors involved in cool-season grass response to high soil temperature. *Environmental and Experimental Botany*, **53**, 233–245.

McGregor, N., Yin, N., Tung, C.C., Van Petegem, F. & Brumer, H. (2017) Crystallographic insight into the evolutionary origins of xyloglucan endotransglycosylases and endohydrolases. *The Plant Journal*, **89**, 651–670.

Mellerowicz, E.J., Immerzeel, P. & Hayashi, T. (2008) Xyloglucan: the molecular muscle of trees. *Annals of Botany*, **102**, 659–665.

Miedes, E., Suslov, D., Vandenbussche, F., Kenobi, K., Ivakov, A., Van Der Straeten, D. *et al.* (2013) Xyloglucan endotransglucosylase/hydrolase (XTH) overexpression affects growth and cell wall mechanics in etiolated Arabidopsis hypocotyls. *Journal of Experimental Botany*, **64**, 2481–2497.

Mohler, K.E., Simmons, T.J. & Fry, S.C. (2013) Mixed-linkage glucan:xyloglucan endotransglucosylase (MXE) re-models hemicelluloses in *Equisetum* shoots but not in barley shoots or *Equisetum* callus. *New Phytologist*, **197**, 111–122.

Ndamukong, I., Chetram, A., Saleh, A. & Avramova, Z. (2009) Wall-modifying genes regulated by the Arabidopsis homolog of trithorax, ATX1: repression of the XTH33 gene as a test case. *The Plant Journal*, **58**, 541–553.

Nelson, B.K., Cai, X. & Nebenführ, A. (2007) A multicolored set of in vivo organelle markers for co-localization studies in Arabidopsis and other plants. *The Plant Journal*, **51**, 1126–1136.

Nishitani, K. & Vissenberg, K. (2006) Roles of the XTH protein family in the expanding cell. In: Verbelen, J.P. & Vissenberg, K. (Eds.) *The expanding cell. Plant cell monographs*. **6**, Berlin, Heidelberg: Springer, pp. 89–116.

Park, Y.B. & Cosgrove, D.J. (2012) Changes in cell wall biomechanical properties in the xyloglucan-deficient *xxt1/xxt2* mutant of Arabidopsis. *Plant Physiology*, **158**, 465–475.

Park, Y.B. & Cosgrove, D.J. (2015) Xyloglucan and its interactions with other components of the growing cell wall. *Plant Cell Physiology*, **56**, 180–194.

Pinedo, M., Regente, M., Elizalde, M., Quiroga, I.Y., Pagnussat, L.A., Jorrin-Novo, J. *et al.* (2012) Extracellular sunflower proteins: evidence on non-classical secretion of a jacalin-related lectin. *Protein and Peptide Letters*, **19**, 270–276.

Popper, Z.A. & Fry, S.C. (2008) Xyloglucan-pectin linkages are formed intraprotoplasmically, contribute to wall-assembly, and remain stable in the cell wall. *Planta*, **227**, 781–794.

Poulsen, C.P., Dilokpimol, A., Mouille, G., Burow, M. & Geshi, N. (2014) Arabinogalactan glycosyltransferases target to a unique subcellular compartment that may function in unconventional secretion in plants. *Traffic*, **15**, 1219–1234.

Regente, M., Pinedo, M., Elizalde, M. & de la Canal, L. (2012) Apoplastic exosome-like vesicles: a new way of protein secretion in plants? *Plant Signaling and Behavior*, **7**, 544–546.

Rehman, R.U., Stigliano, E., Lycett, G.W., Sticher, L., Sbano, F., Faraco, M. *et al.* (2008) Tomato Rab11a characterization evidenced a difference between SYP121-dependent and SYP122-dependent exocytosis. *Plant Cell Physiology*, **49**, 751–766.

Robinson, D.G., Ding, Y. & Jiang, L. (2016) Unconventional protein secretion in plants: a critical assessment. *Protoplasma*, **253**, 31–43.

Rose, J.K., Braam, J., Fry, S.C. & Nishitani, K. (2002) The XTH family of enzymes involved in xyloglucan endotransglucosylation and endohydrolysis: current perspectives and a new unifying nomenclature. *Plant Cell Physiology*, **43**, 1421–1435.

Saeed, B., Brillada, C. & Trujillo, M. (2019) Dissecting the plant exocyst. *Current Opinion in Plant Biology*, **52**, 69–76.

Scheller, H.V. & Ulvskov, P. (2010) Hemicelluloses. *Annual Reviews in Plant Biology*, **61**, 263–289.

Schmittgen, T.D. & Livak, K.J. (2008) Analyzing real-time PCR data by the comparative C(T) method. *Nature Protocols*, **3**, 1101–1108.

Schultink, A., Liu, L., Zhu, L. & Pauly, M. (2014) Structural diversity and function of xyloglucan sidechain substituents. *Plants*, **3**, 526–542.

Shinohara, N., Sunagawa, N., Tamura, S., Yokoyama, R., Ueda, M., Igarashi, K. *et al.* (2017) The plant cell-wall enzyme AtXTH3 catalyses covalent cross-linking between cellulose and cello-oligosaccharide. *Science Reports*, **7**, 46099.

Simmons, T.J. & Fry, S.C. (2017) Bonds broken and formed during the mixed-linkage glucan: Xyloglucan endotransglucosylase reaction catalysed by *Equisetum* hetero-trans-β-glucanase. *Biochemical Journal*, **474**, 1055–1070.

Simmons, T.J., Mohler, K.E., Holland, C., Goubet, F., Franková, L., Houston, D.R. *et al.* (2015) Hetero-trans-β-glucanase, an enzyme unique to Equisetum plants, functionalizes cellulose. *The Plant Journal*, **83**, 753–769.

Sinclair, R., Rosquete, M.R. & Drakakaki, G. (2018) Post-Golgi trafficking and transport of cell wall components. *Frontiers in Plant Science*, **9**, 1784.

Tan, L., Eberhard, S., Pattathil, S., Warder, C., Glushka, J., Yuan, C. *et al.* (2013) An Arabidopsis cell wall proteoglycan consists of pectin and arabinoxylan covalently linked to an arabinogalactan protein. *The Plant Cell*, **25**, 270–287.

Thompson, J.E. & Fry, S.C. (2001) Restructuring of wall-bound xyloglucan by transglycosylation in living plant cells. *The Plant Journal*, **26**, 23–34.

Van Sandt, V.S., Guisez, Y., Verbelen, J.P. & Vissenberg, K. (2006) Analysis of a xyloglucan endotransglycosylase/hydrolase (XTH) from the lycopodiophyte *Selaginella kraussiana* suggests that XTH sequence characteristics and function are highly conserved during the evolution of vascular plants. *Journal of Experimental Botany*, **57**, 2909–2922.

Vissenberg, K., Martinez-Vilchez, I.M., Verbelen, J.-P., Miller, J.G. & Fry, S.C. (2000) In vivo colocalization of xyloglucan endotransglycosylase activity and its donor substrate in the elongation zone of Arabidopsis roots. *The Plant Cell*, **12**, 1229–1237.

Wang, J., Ding, Y., Wang, J., Hillmer, S., Miao, Y., Lo, S.W. *et al.* (2010) EXPO, an exocyst-positive organelle distinct from multivesicular endosomes and autophagosomes, mediates cytosol to cell wall exocytosis in Arabidopsis and tobacco cells. *The Plant Cell*, **22**, 4009–4030.

Wang, T., Park, Y.B., Caporini, M.A., Rosay, M., Zhong, L., Cosgrove, D.J. & *et al.* (2013) Sensitivity-enhanced solid-state NMR detection of expansin's target in plant cell walls. *Proceedings of the National Academy of Sciences of the United States of America*, **110**, 16444–16449.

Wang, X., Chung, K.P., Lin, W. & Jiang, L. (2017) Protein secretion in plants: Conventional and unconventional pathways and new techniques. *Journal of Experimental Botany*, **69**, 21–37.

Xiao, C., Zhang, T., Zheng, Y., Cosgrove, D.J. & Anderson, C.T. (2016) Xyloglucan deficiency disrupts microtubule stability and cellulose biosynthesis in *Arabidopsis*, altering cell growth and morphogenesis. *Plant Physiology*, **170**, 234–249.

Yang, L., Wang, C.C., Guo, W.D., Li, X.B., Lu, M. & Yu, C.L. (2006) Differential expression of cell wall related genes in the elongation zone of rice roots under water deficit. *Russian Journal of Plant Physiology*, **53**, 390–395.

Yokoyama, R. & Nishitani, K. (2001a) A comprehensive expression analysis of all members of a gene family encoding cell-wall enzymes allowed us to predict cis-regulatory regions involved in cell-wall construction in specific organs of Arabidopsis. *Plant Cell Physiology*, **42**, 1025–1033.

Yokoyama, R. & Nishitani, K. (2001b) Endoxyloglucan transferase is localized both in the cell plate and in the secretory pathway destined for the apoplast in tobacco cells. *Plant Cell Physiology*, **42**, 292–300.

Zárský, V., Cvrcková, F., Potocký, M. & Hála, M. (2009) Exocytosis and cell polarity in plants - exocyst and recycling domains. *New Phytologist*, **183**, 255–272.

Zárský, V., Sekereš, J., Kubátová, Z., Pečenková, T. & Cvrčková, F. (2020) Three subfamilies of exocyst EXO70 family subunits in land plants: early divergence and ongoing functional specialization. *Journal of Experimental Botany*, **71**, 49–62.

Zhang, H., Zhang, L., Gao, B., Fan, H., Jin, J., Botella, M.A. *et al.* (2011) Golgi apparatus-localized synaptotagmin 2 is required for unconventional secretion in Arabidopsis. *PLoS One*, **6**, e26477.

Zheng, Y., Wang, X., Chen, Y., Wagner, E. & Cosgrove, D.J. (2018) Xyloglucan in the primary cell wall: assessment by FESEM, selective enzyme digestions and nanogold affinity tags. *The Plant Journal*, **92**, 211–226.

Zhu, X.F., Shi, Y.Z., Lei, G.J., Fry, S.C., Zhang, B.C., Zhou, Y.H. *et al.* (2012) XTH31, encoding an in vitro XEH/XET-active enzyme, regulates aluminum sensitivity by modulating in vivo XET action, cell wall xyloglucan content, and aluminum binding capacity in Arabidopsis. *The Plant Cell*, **24**, 4731–4747.

Zhu, X.F., Wan, J.X., Sun, Y., Shi, Y.Z., Braam, J., Li, G.X. *et al.* (2014) Xyloglucan endotransglucosylase-hydrolase17 interacts with xyloglucan endotransglucosylase-hydrolase31 to confer xyloglucan endotransglucosylase action and affect aluminum sensitivity in *Arabidopsis*. *Plant Physiology*, **165**, 1566–1574.

Zinchuk, V., Zinchuk, O. & Okada, T. (2007) Quantitative colocalization analysis of multicolor confocal immunofluorescence microscopy images: Pushing pixel to explore biological phenomena. *Acta Histochemica et Cytochemica*, **40**, 101–111.